Rheology of bidisperse granular mixtures via event-driven simulations

By MEHEBOOB ALAM[1] AND STEFAN LUDING[1,2]

[1]Institut für Computeranwendungen 1, Pfaffenwaldring 27, 70569 Stuttgart, Germany

[2]Particle Technology, DelftChemTech, TU-Delft, Julianalaan 136,
2628 BL Delft, The Netherlands

The bulk rheology of bidisperse mixtures of granular materials is examined under homogeneous shear flow conditions using the event-driven simulation method. The granular material is modelled as a system of smooth inelastic disks, interacting via the hard-core potential. In order to understand the effect of size and mass disparities, two cases were examined separately, namely, a mixture of different sized particles with particles having either the same mass or the same material density. The relevant macroscopic quantities are the pressure, the shear viscosity, the granular energy (fluctuating kinetic energy) and the first normal stress difference.

Numerical results for pressure, viscosity and granular energy are compared with a kinetic-theory constitutive model with excellent agreement in the low dissipation limit even at large size disparities. Systematic quantitative deviations occur for stronger dissipations. Mixtures with equal-mass particles show a stronger shear resistance than an equivalent monodisperse system; in contrast, however, mixtures with equal-density particles show a reduced shear resistance. The granular energies of the two species are unequal, implying that the equipartition principle assumed in most of the constitutive models does not hold. Inelasticity is responsible for the onset of energy non-equipartition, but mass disparity significantly enhances its magnitude. This lack of energy equipartition can lead to interesting non-monotonic variations of the pressure, viscosity and granular energy with the mass ratio if the size ratio is held fixed, while the model predictions (with the equipartition assumption) suggest a monotonic behaviour in the same limit. In general, the granular fluid is non-Newtonian with a measurable first normal stress difference (which is positive if the stress is defined in the compressive sense), and the effect of bidispersity is to increase the normal stress difference, thus enhancing the non-Newtonian character of the fluid.

1. Introduction

Granular media consist of a collection of discrete macroscopic solid particles, interacting via short-range repulsive contact forces; common examples of granular materials include sand, gravel, sugar, salt, cereals and powders. The behaviour of granular materials is of immense importance in many industrial and geological processes; most agricultural and pharmaceutical products are in granular form. In a typical 'dry' granular flow, particle–particle interactions are inherently dissipative and this, in turn, leads to a wealth of interesting and unresolved behaviour (Herrmann, Hovi & Luding 1998). Despite their practical importance and non-trivial dynamics, the understanding of granular materials still remains poor. While the constitutive models based on the kinetic theory of dense gases have been reasonably successful in

describing the 'rapid-shear' fluidized regime, much work is needed on the 'intermediate' regimes where fluidized states coexist with non-deforming solid-like states. Currently there is no consensus on the status of a continuum theory that can describe the whole range of intriguing behaviour of real granular systems.

Apart from experiments, there are two complementary approaches to research on particulate flows (see, for example, Campbell 1990; Behringer & Jenkins 1997; Herrmann *et al.* 1998; Pöschel & Luding 2001; Kishino 2001). The development of continuum theories, on the one hand, is nicely complemented by discrete particle simulations on the other hand. For a numerical/analytical solution of the partial differential equations of mass, momemtum and energy balance from the continuum theory, we need to have proper constitutive models at our disposal, but their development, even for a dilute system of inelastic hard spheres, is not a trivial task (Sela & Goldhirsch 1998). However, certain 'minimal' models can be developed or postulated using ideas from statistical mechanics (Haff 1983; Jenkins & Savage 1983; Lun *et al.* 1984; Jenkins & Richman 1985; Goldshtein & Shapiro 1995; van Noije & Ernst 1998; Savage 1998; Luding *et al.* 1998). Direct simulations of these continuum models help to probe the range of validity of such models by comparing simulation data with numerical experiments. From the point of view of discrete-particle simulations, the goal is to predict and verify the rheological equations of state for pressure, viscosity, thermal conductivity, etc. considering 'model' systems. In particular, the standard hard-sphere model taking into account the dissipative nature of particle collisions has been successful in simulating the dynamics of granular materials in the rapid-shear regime (Campbell 1990; Pöschel & Luding 2001); furthermore, this model serves as a test-bed to verify the kinetic-theory-based constitutive relations. In the last two decades, such studies have greatly improved our understanding about the rheological behaviour and microstructural features of granular materials (Herrmann *et al.* 1998).

The majority of the rheological studies on granular materials are confined to monodisperse systems, where the particles are of the same density and size. A real granular system is always characterized by some degrees of polydispersity in density and size, which often leads to unwanted segregation (Hong, Quinn & Luding 2001) of an otherwise homogeneous mixture, for example, in powder processing (Chowhan 1995). Apart from size disparity, one should also take into account other important features like Coulomb friction, roughness, and non-sphericity of particles, etc. to truly model a real granular system (Louge 1994; Lun & Bent 1994; Luding *et al.* 1998). The natural starting point to understand the effects of polydispersity on the bulk rheology of the mixture is to focus first on a bidisperse system of smooth inelastic hard spheres under homogeneous shear deformation. This is the first objective of our work, i.e. to understand the bulk rheology of the mixture and the influence of various system control parameters on it. Such knowledge on the rheology will help to make meaningful progress in developing better constitutive models.

Following the analogy with dense-gas kinetic theory of mixtures (Ferziger & Kaper 1972; Lopez de Haro, Cohen & Kincaid 1983), constitutive models for bidisperse granular mixtures were proposed by Jenkins & Mancini (1987, 1989) about a dozen years ago, with important modifications being recently incorporated by Arnarson & Willits (Arnarson & Willits 1998; Willits & Arnarson 1999). Based on their constitutive model, Jenkins & Mancini (1989) showed that steady, fully developed flow with an imposed gradient in particle fluctuation energy ('granular' energy) would lead to size segregation. This idea has recently been tested by performing microgravity experiments of bidisperse mixtures in a shear cell (Louge *et al.* 2001). In conjunction

with experiments, Louge *et al.* also performed discrete-particle simulations for hard-sphere mixtures in a similar setup. Both their experimental and simulation results on flow properties like solid fraction, mean velocity and fluctuation energy compare very well with the predictions of their constitutive model. It should be mentioned that the experiments, as well as their simulations, were performed for particles with a small size-ratio of about 1.25 and a coefficient of restitution in the range 0.93–0.97.

Before using any constitutive model for large-scale simulations (Nott *et al.* 1999) or as a predictive tool, it is important to know its range of validity in terms of all the control parameters (e.g. inelasticity, size ratio, solid fraction, etc.) as well as the validity of some of the underlying assumptions. This forms the second objective of our work, i.e. to compare the rheological data obtained from simulations with predictions of the constitutive model in a wide parameter space and to pinpoint the limitations of such models. Some effort in this direction has been made by Luding & Strauß (2001; Strauß 1999) who carried out event-driven simulations for bi- and polydisperse granular mixtures in the freely cooling state, and obtained a global equation of state for pressure valid in the whole of range of solid fraction. Among many interesting findings, their work showed that the principle of equipartition of granular energy does not hold as the inelasticity and the size ratio increase as also reported more recently by Montanero & Garzo (2002).

The current work represents a systematic computer simulation study in two dimensions to probe the rheological behaviour of a binary granular mixture, where the particles differ in size and mass. We use the familiar smooth hard-disk model for an event-driven simulation (Allen & Tildesley 1989) of the uniform shear flow configuration. The details of the simulation and the model system are described in §2. The macroscopic quantities that we calculate are the pressure, the shear viscosity, the granular energy and the first normal stress difference, also introduced in detail in §2. For the uniform shear flow, a kinetic-theory-based constitutive model (Jenkins & Mancini 1987; Willits & Arnarson 1999; Alam *et al.* 2002) is used to derive the analytical expressions for these macroscopic quantities, as described in §3. In §4 the results for the monodisperse case are presented, verifying earlier results and benchmarking our simulation code. We have carried out simulations for two kinds of bidisperse mixtures as detailed in §5. The results for the equal-mass mixture, for which the particles differ only in size but their masses are equal, are presented in §5.1. The results for the other case of an equal-density mixture, for which the particles are made of the same material but differ in size and thus in mass, are presented in §5.2. The issue of the equipartition of granular energy is examined more closely in §6.1 by comparing our simulation results to available experimental and theoretical data. The possible impact of the equipartition assumption in predicting the transport coefficients at large mass disparities is discussed §6.2. In §7 we summarize our findings with suggestions for possible future work.

2. Numerical simulations

We consider a collection of smooth inelastic hard disks in a square box of size $\tilde{L}$ under uniform shear flow; let $\tilde{x}$ and $\tilde{y}$ be the streamwise and transverse directions, respectively, with the origin of the coordinate frame positioned at the centre of the box. A typical snapshot of the simulation is shown in figure 1(*a*). Note that dimensional quantities are denoted by tildes, whereas the non-dimensional quantities are without. The reference length, time, and velocity scales for non-dimensionalization will be specified later in this section.
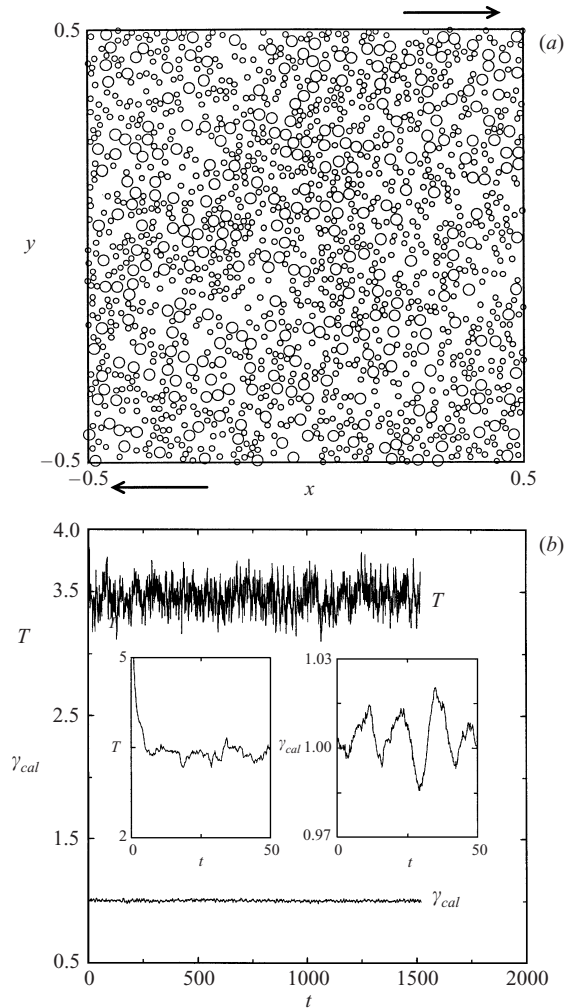
FIGURE 1. (*a*) A snapshot of the sheared bidisperse granular mixture at steady state. The arrows indicate the displacement of the image boxes. (*b*) Variations of the granular energy T and the calculated shear rate γ_{cal} with time. For an explanation of the system and particle properties, see text. The parameters for (*a*) and (*b*) are $v = 0.3$, $\chi = 0.5$, $R = 2$, $N_l = 300$, $N_s = 1200$, $m_l = m_s$ and $e = 0.9$.

2.1. *Contacts and algorithm*

Since the rapid-shear regime is of interest here, the interaction model is the classical hard-disk model and the algorithm is event-driven (ED) molecular dynamics.

2.1.1. *Collision model for hard disks*

In the following, we shall denote the quantities associated with the species of larger size with suffix l and those of smaller size with suffix s. Let the diameter and the mass of particle i be $\tilde{d}_i$ and $\tilde{m}_i$, respectively. The reduced mass for a pair of particles i and j is defined as

$$\tilde{\mu}_{ij} = \frac{\tilde{m}_i \tilde{m}_j}{\tilde{m}_i + \tilde{m}_j},$$

so that

$$M_{ij} = \frac{\tilde{\mu}_{ij}}{\tilde{m}_j} = \frac{\tilde{m}_i}{\tilde{m}_i + \tilde{m}_j},$$

with $\tilde{\mu}_{ii} = \tilde{m}_i/2$ and $M_{ii} = 1/2$. The pre- and post-collisional velocities of particle i are denoted by $\tilde{c}_i$ and $\tilde{c}'_i$, respectively. The velocity of particle j relative to i is $\tilde{c}_{ji} = \tilde{c}_j - \tilde{c}_i$. Let $\boldsymbol{k}_{ji} = \boldsymbol{k}$ be the unit vector directed from the center of the particle j to that of particle i. The pre- and post-collisional velocities are related by the expression:

$$\boldsymbol{k} \cdot \tilde{\boldsymbol{c}}'_{ji} = -e_{ij}(\boldsymbol{k} \cdot \tilde{\boldsymbol{c}}_{ji}), \tag{2.1}$$

where e_{ij} is the coefficient of normal restitution between particles i and j, with $e_{ij} = e_{ji}$ and $0 \leqslant e_{ij} \leqslant 1$. Note that we restrict considerations to perfectly smooth particles and that $e_{ij} = e$ is implied in the following. From the conservation of linear momentum, it immediately follows that

$$\tilde{\boldsymbol{c}}'_i = \tilde{\boldsymbol{c}}_i + M_{ji}(1 + e_{ij})(\boldsymbol{k} \cdot \tilde{\boldsymbol{c}}_{ji})\boldsymbol{k} = \tilde{\boldsymbol{c}}_i - M_{ji}(1 + e_{ij})(\boldsymbol{k} \cdot \tilde{\boldsymbol{c}}_{ij})\boldsymbol{k}, \tag{2.2}$$

with $\boldsymbol{k}_{ji} = -\boldsymbol{k}_{ij}$. The expression for the collisional impulse

$$\tilde{\boldsymbol{I}}_{ij} = \tilde{m}_i(\tilde{\boldsymbol{c}}'_i - \tilde{\boldsymbol{c}}_i) = \tilde{\mu}_{ij}(1 + e_{ij})(\boldsymbol{k} \cdot \tilde{\boldsymbol{c}}_{ji})\boldsymbol{k}, \tag{2.3}$$

directed along $\boldsymbol{k}$, readily follows from (2.2).

2.1.2. *ED-algorithm*

Given the initial positions and velocities of the particles, an event-driven algorithm is used to simulate the instantaneous binary collisions, which means solving a quadratic polynomial for the collision time. To find the potential collision partners (i,j) and their collision times (t_{ij}), only particles that are located within the nearest neighbourhood of the 'test' particle are considered for possible collisions, using the well-known linked-cell algorithm (Allen & Tildesley 1989). After determining the minimum collision time (t_{ij}^{min}), all particle positions are advanced following the well-known kinematic relation and the time is also increased by t_{ij}^{min}. At this point, only two particles are in contact and their velocities are updated by implementing the collision dynamics as described in §2.1.1.

2.2. *Model system*

The system is periodic in the $\tilde{x}$-direction, i.e. a particle crossing the left/right boundary re-enters the system through the opposite boundary at the same vertical position with unchanged velocities. To impose a uniform shear rate ($\tilde{\gamma} = \tilde{U}/\tilde{L}$) in the $\tilde{y}$-direction, the top and bottom image boxes, bounding the computational box, are set in motion with velocities $\tilde{U}/2$ and $-\tilde{U}/2$, respectively, in the streamwise direction. The velocity jump ($\tilde{U}$) between the top and bottom boundaries and the non-stationary nature of the image boxes are taken into account by using the so-called Lees–Edwards boundary condition (Lees & Edwards 1972), which mimics the state of uniform shear flow (USF) by imparting momemtum transfer by shearing.

2.2.1. *Control parameters*

It is appropriate at this point to identify the relevant dimensionless parameters for our simulated system. The reference length, time, velocity and mass are $\tilde{L}$, $\tilde{\gamma}^{-1}$, $\tilde{\gamma}\tilde{L}$ and $\tilde{m}_l$. Thus the simulation box spans the range $[-0.5, 0.5]$ in both streamwise and transverse directions; the top image-box moves with a velocity of 0.5 and the bottom with -0.5, see figure 1(a). There are six dimensionless control parameters:

the total solid volume fraction (v), the relative volume fraction of larger particles ($\chi = \chi_l = v_l/v$), the size ratio ($R = R_{ls} = \tilde{d}_l/\tilde{d}_s \geqslant 1$), the dimensionless diameter of the larger particle (d_l), the mass ratio (m_l/m_s), and the coefficient of normal restitution (e). The imposed shear rate γ is kept fixed at unity in the simulations since its variation by an order of magnitude does not influence the reported results.

Note that $\chi = 1$ and $\chi = 0$ correspond to the monodisperse limits with all particles being large or small, respectively. We have restricted the present study to solid volume fractions $v \leqslant 0.6$, well below the freezing-point value of $v \approx 0.70$ in two-dimensions (Luding & Strauß 2001; Luding 2001). For given v and χ, the number of particles (N_l and N_s) can be computed by knowing the size ratio R and the diameter of the large particles. For most of the simulations, we fixed $d_l = 0.025\,23$, which corresponds to a box length of about 40 large-particle diameters. The simulations are carried out for the coefficient of restitution $e \geqslant 0.5$ and for size ratios $R \leqslant 5$. The dependence of the measured quantities on the system size was considered for a few cases.

2.2.2. *Initial configuration and steady state*

In a typical simulation, the particles are placed into the system randomly and their mean horizontal flow velocity is determined by their vertical position. In addition to this shear flow, a random Gaussian velocity component is added to all velocity components. The simulation is then started by specifying the restitution coefficient ($e < 1$).

To ascertain whether the system has reached the statistical steady state, the time evolution of the average fluctuation kinetic energy ('granular energy') is monitored, see figure 1(b). Unlike in a purely elastic system, where shear leads to continual heating, the fluctuation kinetic energy saturates to a constant value after the initial transient, a consequence of the balance between the shear work and the collisional dissipation. Depending on the value of the coefficient of restitution and the total number of particles, it can take up to 1000 collisions per particle to reach such a statistical steady state – the lower the value of e and/or the smaller the value of N, the faster the system reaches the steady state and vice versa. The simulation is then allowed to run for another 4000–5000 collisions per particle to gather data to calculate the rheological quantities. A few longer runs (10 000 collisions per particle) were also checked, with no significant change in the measured macroscopic quantities. Another quantity which was simultaneously monitored, along with the granular energy, is the linearity of the streamwise velocity profile across the Couette gap, and we found that the calculated shear rate (i.e. the slope of the velocity profile) fluctuated around the imposed shear rate by at most 0.5%. The instantaneous shear rate (see figure 1b) was calculated by binning the system into equal-size bins in the transverse direction, and then taking appropriate averages over all the particles in each bin.

We looked closer at the effect of the initial particle configurations by considering ordered configurations in which the larger particles were placed above the smaller particles. Even though it took longer to attain the steady state, the measured macroscopic quantities did not differ noticeably from those for random initial particle configurations.

2.3. *Macroscopic quantities*

On making a transition from the microscale to the macroscale, we encounter broadly two kinds of macroscopic quantities: mean fields (or flow properties) and rheological quantities. The mean fields are solid fraction, velocity and higher-order field variables (e.g. granular energy), each suitably averaged. For the uniform shear flow, the defor-

mation is homogeneous and hence the mean fields (except the streamwise velocity which varies linearly with the transverse coordinate) are uniform in the computational box, as verified in our simulations. (For dense quasi-static shear flow, characterized by inhomogeneous deformation, the mean fields are non-uniform and the averaging procedure is much more involved (Lätzel, Luding & Herrmann 2000).) Thus, we mainly focus on the rheological properties of the homogeneous granular mixture, i.e. the macroscopic stress and its related surrogates (pressure, shear viscosity, and the first normal stress difference).

With $\tilde{L}$, $\tilde{\gamma}^{-1}$, $\tilde{\gamma}\tilde{L}$ and $\tilde{m}_l$, used as the reference length, time, velocity and mass, respectively, the relevant dimensionless quantities are

$$
\left.
\begin{aligned}
d_i = \frac{\tilde{d}_i}{\tilde{L}}, \quad m_i = \frac{\tilde{m}_i}{\tilde{m}_l}, \quad (c_i, \boldsymbol{u}, C_i) = \frac{1}{\tilde{\gamma}\tilde{L}}(\tilde{c}_i, \tilde{\boldsymbol{u}}, \tilde{C}_i), \\
\boldsymbol{P} = \frac{\tilde{\boldsymbol{P}}}{\tilde{\gamma}^2 \sum\limits_{\alpha=l,s} \chi_\alpha \tilde{\rho}_\alpha \tilde{d}_\alpha^2}, \quad T = \frac{\tilde{T}}{\tilde{\gamma}^2 \sum\limits_{\alpha=l,s} \chi_\alpha \tilde{m}_\alpha \tilde{d}_\alpha^2},
\end{aligned}
\right\}
\tag{2.4}
$$

where $\boldsymbol{u}$ is the mass-averaged ('hydrodynamic') velocity, $C_i = c_i - \boldsymbol{u}$ the fluctuation velocity of particle i, $\tilde{\rho}_\alpha$ the material density of species α, $\boldsymbol{P}$ the total stress tensor, and T the granular energy of the mixture (defined below). The stress is thus rescaled by the species-averaged momentum flux density, whereas the granular energy is rescaled by the species-averaged kinetic energy.

The macroscopic stress, as measured in discrete particle simulations, is a byproduct of the particle-level mechanisms of momemtum transfer. The total stress is the sum of two different parts, kinetic stress and collisional stress. The 'kinetic' stress arises from the momentum transport due to the fluctuating motion of the particles, while the momentum transport due to the interparticle collisions is responsible for the 'collisional' mode of stress.

2.3.1. *Kinetic stress contribution*

By analogy with a molecular gas, the kinetic contribution to the partial stress tensor (or species stress tensor) is calculated from

$$
\tilde{\boldsymbol{P}}_\alpha^k = \langle \tilde{\rho}_\alpha \tilde{C}_\alpha \tilde{C}_\alpha \rangle = \tilde{\rho}_l \nu_\alpha \frac{1}{N_\alpha} \sum_{i=1}^{N_\alpha} \tilde{C}_i \tilde{C}_i = \tilde{\rho}_l \tilde{d}_l^2 \tilde{\gamma}^2 \frac{\nu_\alpha}{d_\alpha^2} \left[\frac{m_\alpha}{N_\alpha} \sum_{i=1}^{N_\alpha} C_i C_i \right]
$$

$$
\Rightarrow \boldsymbol{P}_\alpha^k = \frac{\tilde{\boldsymbol{P}}_\alpha^k}{\tilde{\gamma}^2 \sum\limits_{\alpha=l,s} \chi_\alpha \tilde{\rho}_\alpha \tilde{d}_\alpha^2} = \frac{\pi}{4 \sum\limits_{\alpha=l,s} (\rho_\alpha/\rho_l)\chi_\alpha R_{\alpha l}^2} \left[m_\alpha \sum_{i=1}^{N_\alpha} C_i C_i \right],
\tag{2.5}
$$

where the angular brackets $\langle\ldots\rangle$ denote the appropriate volume averaging. The total kinetic stress is obtained by just summing the partial components:

$$
\boldsymbol{P}^k = \sum_{\alpha=l,s} \boldsymbol{P}_\alpha^k.
\tag{2.6}
$$

From here onwards the greek indices (α, β, ...) denote a species (l or s), while the arabic indices (i, j, ...) denote single particles if summation is necessary.

2.3.2. *Collisional stress contribution*

Due to the instantaneous nature of hard-core collisions, each collision results in a momemtum exchange equal to the collisional impulse $\tilde{\boldsymbol{I}}_{ij}$, as defined in equation (2.3). The effect of a collision is the transport of $\tilde{\boldsymbol{I}}_{ij}$ over a distance $(\tilde{d}_i + \tilde{d}_j)/2$ in the direction of $\boldsymbol{k}$. Thus the collisional part of the stress tensor is calculated from

$$\tilde{\boldsymbol{P}}^c = \frac{1}{2\tilde{L}^2\tau_d}\sum_{\text{coll.}}(\tilde{d}_i + \tilde{d}_j)(\tilde{\boldsymbol{I}}_{ij} \otimes \boldsymbol{k}) = \frac{\tilde{\rho}_l\tilde{d}_l^2\tilde{\gamma}^2}{2\tau_d}\sum_{\text{coll.}}(d_i + d_j)(\boldsymbol{I}_{ij} \otimes \boldsymbol{k})$$

$$\Rightarrow \boldsymbol{P}^c = \frac{\tilde{\boldsymbol{P}}^c}{\tilde{\gamma}^2\sum_{\alpha=l,s}\chi_\alpha\tilde{\rho}_\alpha\tilde{d}_\alpha^2} = \frac{\pi}{8\tau_d\sum_{\alpha=l,s}(\rho_\alpha/\rho_l)\chi_\alpha R_{\alpha l}^2}\sum_{\text{coll.}}(d_i + d_j)(\boldsymbol{I}_{ij} \otimes \boldsymbol{k}), \qquad (2.7)$$

where τ_d is the duration of the averaging time window and the sum is taken over all collisions during τ_d, where the particles i and j are involved. Clearly, $\boldsymbol{P}^c = \boldsymbol{P}_l^c + \boldsymbol{P}_s^c = \boldsymbol{P}_{ll}^c + \boldsymbol{P}_{ss}^c + \boldsymbol{P}_{ls}^c + \boldsymbol{P}_{sl}^c$ has two contributions for each of the two species: one from the collisions between particles of the same species and the other from collisions between particles of different species. Note that while the kinetic stress (2.5) involves only volume averaging, the collisional stress (2.7) involves both volume and time averaging.

2.3.3. *Pressure, shear stress and viscosity*

The total stress, defined in the compressive sense, may be decomposed in the standard way:

$$\boldsymbol{P} = \sum_{\alpha=l,s}(\boldsymbol{P}_\alpha^k + \boldsymbol{P}_\alpha^c) = p\boldsymbol{1} + \boldsymbol{\Pi}, \qquad (2.8)$$

where p is the pressure, $\boldsymbol{\Pi}$ the pressure deviator and $\boldsymbol{1}$ the unit tensor. From the off-diagonal components of the pressure deviator, we can calculate the shear viscosity which relates the shear stress to the rate of strain:

$$\tilde{\Pi}_{xy} = -\tilde{\mu}\frac{d\tilde{u}}{d\tilde{y}}$$

$$\Rightarrow \mu = \frac{\tilde{\mu}}{\tilde{\gamma}\sum_{\alpha=l,s}\chi_\alpha\tilde{\rho}_\alpha\tilde{d}_\alpha^2} = \frac{-\tilde{\Pi}_{xy}}{\tilde{\gamma}^2\sum_{\alpha=l,s}\chi_\alpha\tilde{\rho}_\alpha\tilde{d}_\alpha^2} = |\Pi_{xy}|. \qquad (2.9)$$

For the steady uniform shear flow, thus, the dimensionless shear viscosity can also be interpreted as the shear stress, due to our adopted scaling.

2.3.4. *First normal stress difference*

The diagonal components of the pressure deviator could be different from zero, giving rise to an anisotropic stress tensor. The magnitude of the stress anisotropy can be quantified by the first normal stress difference

$$\mathcal{N}_1 = \frac{\Pi_{xx} - \Pi_{yy}}{p}. \qquad (2.10)$$

Note that we have scaled this quantity by pressure to obtain its relative magnitude with respect to pressure. For a standard Newtonian fluid, $\mathcal{N}_1 = 0$ and thus $\mathcal{N}_1$ is also an indicator of the non-Newtonian character of the fluid.

2.3.5. *Granular energy*

The granular energy can be obtained from the trace of the kinetic part of the stress tensor, and the species granular energy is calculated from the following expression:

$$\tilde{T}_\alpha = \tfrac{1}{2}\tilde{m}_\alpha \langle \tilde{\boldsymbol{C}}_\alpha \cdot \tilde{\boldsymbol{C}}_\alpha \rangle = \frac{\tilde{m}_\alpha}{2N_\alpha} \sum_{i=1}^{N_\alpha} \tilde{\boldsymbol{C}}_i \cdot \tilde{\boldsymbol{C}}_i$$

$$\Rightarrow T_\alpha = \frac{\tilde{T}_\alpha}{\tilde{\gamma}^2 \sum_{\alpha=l,s} \chi_\alpha \tilde{m}_\alpha \tilde{d}_\alpha^2} = \frac{1}{2d_l^2 \sum_{\alpha=l,s}(m_\alpha/m_l)\chi_\alpha R_{\alpha l}^2} \left[\frac{m_\alpha}{N_\alpha} \sum_{i=1}^{N_\alpha} \boldsymbol{C}_i \cdot \boldsymbol{C}_i \right]. \qquad (2.11)$$

The total granular energy is $T = \sum_{\alpha=l,s} \xi_\alpha T_\alpha$, where $\xi_\alpha = N_\alpha/N$ is the number fraction of species α.

2.3.6. *Averaging*

Most quantities can be calculated from snapshots, but the collisional contribution to the stress tensor requires additional time averaging, taking into account all collisions in the averaging time window. The collisional impulse (2.3) is calculated for each collision and is used for the computation of the collisional stress that is averaged over time, see equation (2.7).

For the typical simulation in figure 1(*a*) at steady state, after 6×10^6 collisions, the parameters values are $v = 0.3$, $\chi = 0.5$, $R = 2$, $N_l = 300$, $N_s = 1200$, $e = 0.9$ and $m_l/m_s = 1.0$. We observe that the large and small particles are randomly distributed and there is no sign of large-scale size segregation. The variations of the granular energy T and the calculated shear rate γ_{cal} with time are shown in figure 1(*b*), along with corresponding initial variations in two insets. (The data represent the instantaneous values of T and γ_{cal} sampled at a regular interval of 600 collisions – no time averaging is involved here.) It is observed that the granular energy reaches its steady value ($T = 3.462 \pm 0.123$) quickly after the initial transients and the calculated shear rate fluctuates around its imposed value ($\gamma = 1$) by about $\pm 0.35\%$. The fluctuations in both T and γ_{cal} at steady state are due to the finite size of the system and diminish with the number of particles as $N^{-1/2}$.

3. Continuum model: kinetic theory

The balance laws for mass, momentum and granular energy of a binary mixture of granular materials are detailed in the Appendix. These equations must be supplemented by a constitutive model for the stress tensor, the collisional dissipation rate, the heat flux and the diffusion flux. To this end we appeal to the kinetic theory of dense gases, taking into account the inelastic nature of particle collisions. Willits & Arnarson (1999) have recently derived the full constitutive model for a binary mixture of inelastic hard disks, extending an earlier work of Jenkins & Mancini (1987) on the same subject. There are two major assumptions in this model: (i) it is first order in inelasticity, meaning that the constitutive relations are valid for quasi-elastic particles. (ii) the granular energy is equally partitioned between the two species.

For our purpose of probing the steady uniform shear flow, the constitutive relations for pressure, shear viscosity and collisional dissipation rate are taken from Willits & Arnarson (1999). Note that a factor is missing from the coefficient of the Sonine polynomial expansion in Willits & Arnarson (see Appendix; Alam *et al.* 2002), and without this missing factor, the theoretical predictions for pressure,

shear viscosity and their partial components can differ in a significant way from the correct values.

3.1. *Shear flow theory*

For the steady $((\partial/\partial t)(.) = 0)$, fully developed $((\partial/\partial x)(.) = 0)$ plane shear flow of a binary mixture of granular materials, it is easy to verify that a linear streamwise velocity profile along with constant solid fraction and constant granular energy satisfies the balance equations. Thus, the mean fields are given by

$$\left.\begin{aligned} v &= \sum_{\alpha=l,s} v_\alpha = \text{const.,} \\ T &= \sum_{\alpha=l,s} \xi_\alpha T_\alpha = \text{const.,} \\ \boldsymbol{u} &\equiv (u,v)^T = (y,0)^T, \end{aligned}\right\} \tag{3.1}$$

where ξ_α is the number fraction of species α. An expression for T can be obtained, for equipartition $T_l = T_s$, from the energy balance equation, by equating the production term due to shear work with collisional dissipation $(\tilde{\mathscr{D}})$:

$$-\tilde{\boldsymbol{P}} : \tilde{\nabla}\tilde{\boldsymbol{u}} = \tilde{\mathscr{D}}$$

$$\Rightarrow T = \frac{\sum_{\alpha=l,s} f_{2\alpha}\sqrt{\rho_\alpha/\rho_l}}{\sum_{\alpha=l,s} f_{5\alpha} R_{l\alpha}^2 (m_l/m_\alpha)\sqrt{\rho_\alpha/\rho_l} \sum_{\beta=l,s} (m_\beta/m_l)\chi_\beta R_{\beta l}^2}, \tag{3.2}$$

with the constitutive relations for $\tilde{\boldsymbol{P}}$ and $\tilde{\mathscr{D}}$ detailed in the Appendix.

The dimensionless expressions for pressure and shear viscosity are

$$p = \sum_{\alpha=l,s} p_\alpha = \frac{T\sum_{\alpha=l,s} f_{1\alpha} \sum_{\beta=l,s}(m_\beta/m_l)\chi_\beta R_{\beta l}^2}{\sum_{\beta=l,s}(\rho_\beta/\rho_l)\chi_\beta R_{\beta l}^2} \tag{3.3}$$

$$\mu = \sum_{\alpha=l,s} \mu_\alpha = \frac{\sqrt{\pi T}\sum_{\alpha=l,s}\sqrt{\rho_\alpha/\rho_l} f_{2\alpha}\sqrt{\sum_{\beta=l,s}(m_\beta/m_l)\chi_\beta R_{\beta l}^2}}{2\sum_{\beta=l,s}(\rho_\beta/\rho_l)\chi_\beta R_{\beta l}^2}, \tag{3.4}$$

where $f_{1\alpha}$ and $f_{2\alpha}$ are functions of the mixture parameters v_α, $R_{\alpha\beta}$, $M_{\alpha\beta}$ etc., as defined in the Appendix.

We will compare our simulation results on pressure, viscosity and granular energy with the predictions of equations (3.3), (3.4) and (3.2), respectively, in the next two sections. For the case of particles of both species having equal mass, the expression for the granular energy reduces to

$$T = \frac{f_{2l} + f_{2s}R}{(f_{5l} + f_{5s}R^3)(\chi_l + \chi_s R^{-2})},$$

and for the case of particles of both species having equal density, the expression for

the granular energy reduces to

$$T = \frac{f_{2l} + f_{2s}}{(f_{5l} + f_{5s}R^4)(\chi_l + \chi_s R^{-4})}.$$

3.2. Low-density limit

The above expressions for pressure, viscosity and granular energy do not show their dependence on the size ratio (R) explicitly since the $f_{n\alpha}$ depend on R in a complicated fashion. To ascertain the correct scaling of p, μ and T with R, it is appropriate to consider the dilute limit ($v \to 0$) for which the expressions for the $f_{n\alpha}$ simplify considerably due to the fact that the radial distribution function tends to unity ($g_{\alpha\beta} \to 1$).

For an equal-mass mixture, the leading-order scalings for pressure, viscosity and granular energy are

$$p = v\chi_s[1 + \tfrac{1}{4}v(1 + e)(\chi_l + 4\chi_s)](\chi_l + \chi_s R^{-2})C_2 R, \tag{3.5}$$

$$\mu = \frac{C_1\sqrt{\pi C_2(\chi_l + \chi_s R^{-2})}}{2}R^{3/2}, \tag{3.6}$$

$$T = C_2 R^{-1}, \tag{3.7}$$

with

$$C_1 = \frac{v^2\chi_l\chi_s}{2\pi}\left[1 + \left(3 + 4\frac{\chi_s}{\chi_l}\right)R^{-1} + O(R^{-2})\right],$$

$$C_2 = \frac{1}{16(1 - e^2)\chi_s}\left[1 + \left(3 + 4\frac{\chi_s}{\chi_l} - \frac{\chi_l}{\chi_s}\right)R^{-1} + O(R^{-2})\right].$$

Thus both the pressure and viscosity increase with growing size ratio and the granular energy decreases in the same limit.

For an equal-density mixture, the leading-order behaviour is

$$p = v\chi_s[1 + \tfrac{1}{4}v(1 + e)(\chi_l + 4\chi_s)]\left(\frac{\chi_l + \chi_s R^{-4}}{\chi_l + \chi_s R^{-2}}\right)C_2 R^{-1}, \tag{3.8}$$

$$\mu = \frac{C_1\sqrt{\pi C_2(\chi_l + \chi_s R^{-4})}}{2(\chi_l + \chi_s R^{-2})}R^{-1/2}, \tag{3.9}$$

$$T = C_2 R^{-3}, \tag{3.10}$$

$$\frac{\mu}{p} = \frac{C_1}{2v\chi_s(1 + (1 + e)\chi_s v)}\sqrt{\frac{\pi}{C_2(\chi_l + \chi_s R^{-2})}}R^{1/2}, \tag{3.11}$$

with

$$C_1 = \frac{v^2\chi_l\chi_s}{\pi\sqrt{2}}\left[1 + \frac{\sqrt{2}(\chi_l^2 + \chi_s^2)}{\chi_l\chi_s}R^{-1} + O(R^{-2})\right],$$

$$C_2 = \frac{1}{16(1 - e^2)\chi_s}\left[1 + \frac{\sqrt{2}(\chi_l^2 + \chi_s^2)}{\chi_l\chi_s}R^{-1} + O(R^{-2})\right].$$

Thus the pressure, viscosity and granular energy all decrease with increasing size ratio. We shall compare these results with simulations in §5.

4. Results: monodisperse system revisited

To compare and contrast the rheology of a bidisperse granular medium with that of its monodisperse counterpart, we first show some results for a monodisperse system over a range of solid fractions and coefficients of restitution. Typical results that follow are the pressure, the shear viscosity, the granular energy, and the first normal stress difference as functions of the solid fraction, the coefficient of restitution, and the system size.

4.1. *Pressure, viscosity and granular energy*

Figure $2(a, b)$ shows a comparison between the pressure and the shear viscosity determined from simulations (symbols) and from kinetic theory (lines) for three different values of the coefficient of restitution. The agreement with the theoretical predictions of Jenkins & Richman (1985) is excellent for both pressure and viscosity in the case $e = 0.99$. Note that the theory underpredicts the simulation data marginally at $v = 0.6$ which may be attributed to our choice of the radial distribution function (A 11) which diverges at $v = 1.0$. By replacing v with v/v_{max} in (A 11) (with $v_{max} = \pi/2\sqrt{3}$ for the maximum regular packing, Luding 2001), we obtain good agreement even at higher solid fractions for $e = 0.99$. The theory overpredicts both p and μ over the whole range of solid fractions for $e = 0.9$, and significant deviations are observed for stronger dissipation $e = 0.7$. This is consistent with the assumptions of the constitutive model which is correct only in the quasi-elastic limit.

The variation of the granular energy with v and e is shown in figure $2(c)$. Again the agreement between theory and simulation is excellent at low dissipation and deteriorates considerably as the dissipation level increases. Note that the granular energy diverges in the dilute limit, and an asymptotic analysis of (3.2) shows $T \sim v^{-2}$. For a physical understanding of the divergent behaviour at low densities, we consider the balance between the shear work and the collisional dissipation term in the energy balance equation (Lun *et al.* 1984; Campbell 1990). Since the shear rate is constant in our simulations, the energy input (shear work) is constant. The collisional dissipation, which balances the shear work, is proportional to the product of the change in fluctuation kinetic energy T and the collision rate. When the solid fraction is decreased, $v \to 0$, the particles have to travel longer paths before a collision occurs and hence the fluctuation velocities (the granular energy) must increase to allow for the dissipation of a fixed amount of input energy. Along the same lines, we note that the divergence of T as $v \to 0$ is also responsible for the divergence of both pressure and viscosity in the same limit, see figures $2(a)$ and $2(b)$. In contrast, the divergence of pressure and viscosity in the dense limit is due to the excluded volume effects and the singular nature of the radial distribution function at contact in the dense limit, see equation (A 11).

To better understand the discrepancy between our simulation results and the theoretical predictions of Jenkins & Richman (1985), we consider another constitutive model of the same authors (Jenkins & Richman 1988) which takes into account the anisotropy in the second moment of the fluctuation velocity. For our purposes, it suffices to focus on the dilute limit. In this limit, the non-dimensional expressions for pressure, viscosity and granular energy can be written as

$$p = vT, \tag{4.1}$$

$$\mu = \sqrt{\delta(1 - \delta)}vT, \tag{4.2}$$

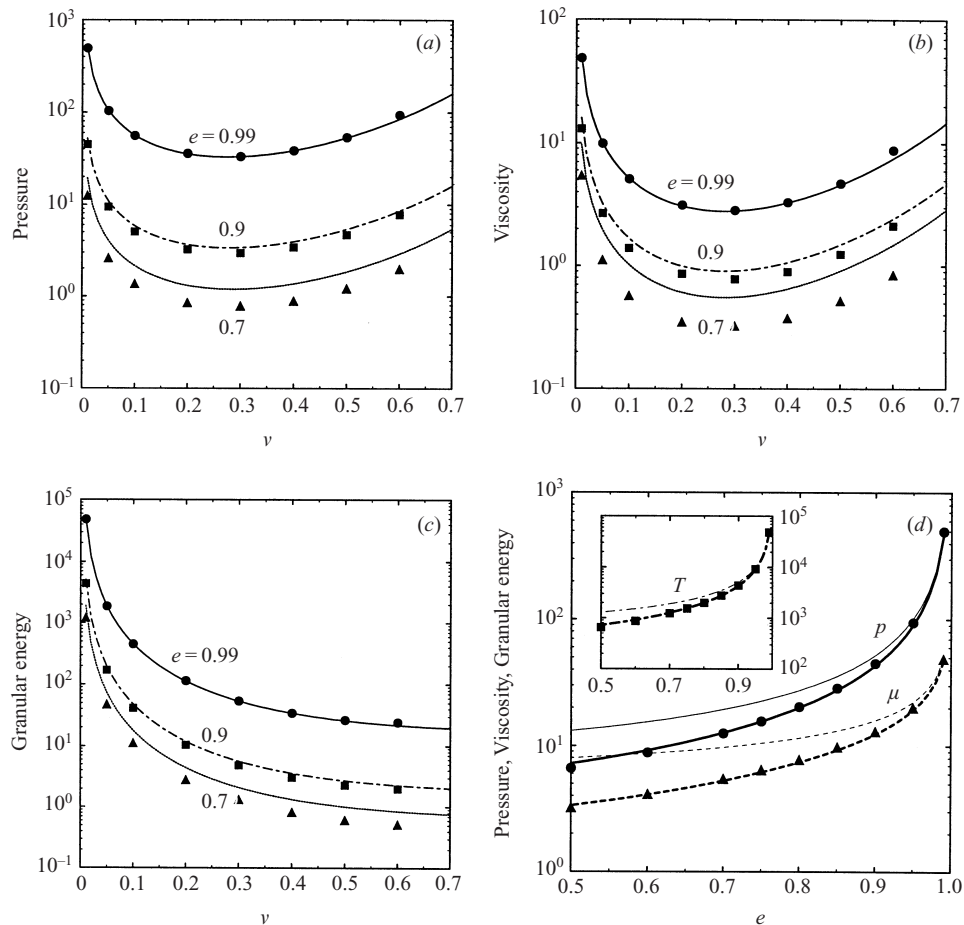$$T = \frac{\pi\delta(1 - \delta)}{16v^2(1 - e^2)^2}, \tag{4.3}$$

FIGURE 2. Variations of (*a*) the pressure, (*b*) the shear viscosity and (*c*) the granular energy with the solid volume fraction for a monodisperse system. The symbols represent simulation data and the lines denote the predictions of the constitutive model of Jenkins & Richman (1985). (*d*) Comparison with the higher-order constitutive model of Jenkins & Richman (1988) in the dilute limit: $v = 0.01$. The thick lines are due to Jenkins & Richman (1988), and the thin lines represent the predictions of their first-order model.

with

$$\delta = \frac{32(1-e)}{16 + 9(1-e)}.$$

Figure 2(*d*) shows the simulation data for p, μ and T, together with the predictions of the above equations denoted by thick lines, and the predictions of the first-order model given by thin lines. Note that the solid fraction is set to 0.01 for this plot. It is observed that the constitutive model of Jenkins & Richman (1988) gives excellent predictions for our rheological data. We may thus conclude that the discrepancies between our simulation results and the theoretical predictions of a first-order model in inelasticity is due to the fact that the latter does not take into account the anisotropy in the second moment of the fluctuation velocity which is a Burnett-order effect (Sela, Goldhirsch & Noskowich 1996).
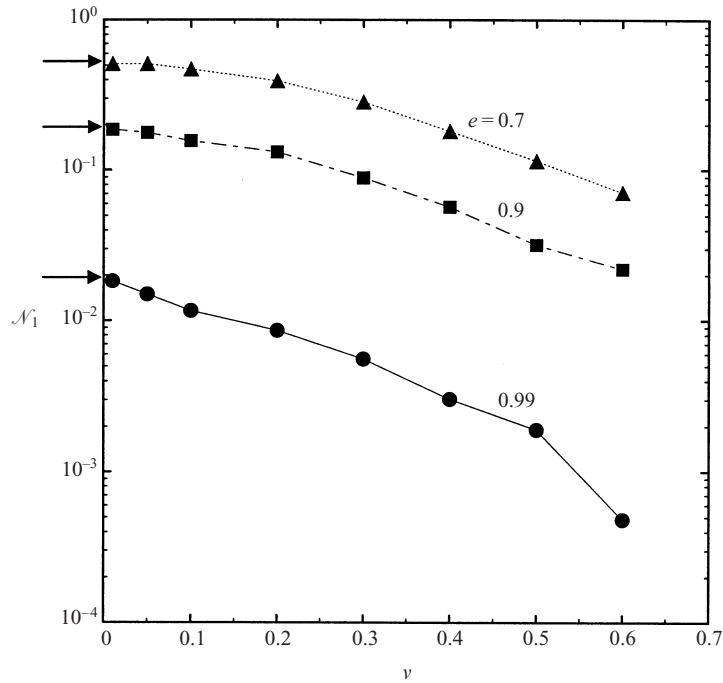
FIGURE 3. Variation of the first normal stress difference $\mathcal{N}_1$ with the solid volume fraction for a monodisperse system. The symbols represent simulation data and the lines are drawn to guide the eye. The arrows on the left ordinate indicate corresponding analytical values for a two-dimensional granular gas (see text for details).

4.2. *Normal stress difference*

It is known from earlier studies (Walton & Braun 1986; Jenkins & Richman 1988; Richman 1989; Campbell 1989, 1990; Hopkins & Louge 1991; Sela *et al.* 1996) that the stress tensor of an inelastic hard-sphere fluid is anisotropic, i.e. there are significant normal stress differences. The variation of the first normal stress difference ($\mathcal{N}_1$) with solid fraction and inelasticity is shown in figure 3. It is observed that $\mathcal{N}_1$ is positive and increases with decreasing v and e, in qualitative agreement with the predictions of Jenkins & Richman (1988). The arrows on the left ordinate indicate the asymptotic values of $\mathcal{N}_1$ for a two-dimensional granular gas in the dilute limit:

$$\mathcal{N}_1 = \begin{cases} \dfrac{32(1-e)}{16+9(1-e)} & \text{(Jenkins \& Richman 1988)} \\ 1.0448(1-e^2) & \text{(Sela \textit{et al.} 1996).} \end{cases} \quad (4.4)$$

(Note that both the expressions yield approximately the same value.) Thus, a small amount of inelasticity makes the stress tensor anisotropic, showing it via a measurable first normal stress difference. It is appropriate to mention here that the limit $e \to 1$ is singular and the normal stress difference survives even in the elastic limit as pointed out by Sela *et al.* (1996). The corresponding expression for $\mathcal{N}_1$ in a molecular gas is:

$$\mathcal{N}_1 \approx 1.358 \frac{\gamma^2 \ell^2}{\langle u^2 \rangle},$$

$\tilde{L}/\tilde{d}$	N	Present data		Hopkins & Louge (1991)	
		Pressure	Viscosity	Pressure	Viscosity
10	38	2.730 (0.010)	0.691 (0.005)	2.730	0.707
21	168	2.897 (0.010)	0.754 (0.006)	2.874	0.754
39.63	600	2.954 (0.004)	0.775 (0.003)	—	—
42	674	2.969 (0.004)	0.779 (0.003)	2.951	0.776
79.26	2400	3.000 (0.007)	0.787 (0.004)	—	—
112.10	4800	3.008 (0.005)	0.788 (0.003)	—	—
198.16	15 000	3.020 (0.020)	0.789 (0.005)	—	—

TABLE 1. Non-dimensional pressure and viscosity ($v = 0.3$, $e = 0.9$).

where ℓ is the mean free path and $\langle u^2 \rangle$ is the r.m.s. of velocity fluctuations. The reason we do not observe normal stress difference in a molecular fluid is that it is extremely small under normal conditions. For example, the magnitude of $\mathcal{N}_1$ for air at room temperature and $\gamma = 1\,\mathrm{s}^{-1}$ is $O(10^{-21})$ and hence $\mathcal{N}_1$ is non-measurable (Sela *et al.* 1996).

We need to point out that while the normal stress differences in the dilute limit arise due to the anisotropy in the second moment of the fluctuation velocity (which is a Burnett-order effect), their origin in the dense limit has recently been tied to the anisotropy in the collision-angle distribution function (Alam & Luding 2002*b*). In particular, it has been shown that the first normal stress difference in a granular fluid can change sign in the dense regime ($v > 0.6$) due to microstructural reorganization of the particles. Similar sign-reversal of $\mathcal{N}_1$ has also been observed in non-Brownian viscous suspensions at high Péclet number (Foss & Brady 2000).

4.3. *System size variation*

In particle-dynamics simulations, one important issue is the dependence of the rheological properties on the system size L, or, equivalently, on the number of particles N. This issue can be directly tied to the existence of a thermodynamic limit for the 'equilibrium' rheological properties. Table 1 shows the variations of pressure and shear viscosity with the system size, along with the corresponding data of Hopkins & Louge (1991) for $v = 0.3$ and $e = 0.9$. Our data extend to much larger systems and represent averages over three independent runs, each starting with a different initial configuration (in terms of particle positions and fluctuation velocities). The value in the parentheses indicates the maximum variation over the mean.

Our results agree well with those of Hopkins & Louge (1991), but both the pressure and the shear viscosity increase with the system size. This dependence of the transport coefficients on the system size has been observed even for perfectly elastic systems (Erpenbeck & Wood 1981). For an inelastic system, however, there are additional effects due to the formation of mobile clusters as the system size increases (Hopkins & Louge 1991; Luding & Herrmann 1999; Liss & Glasser 2001), which may be partly responsible for the significant increase in stress levels in a sheared system. In particular, the recent work of Liss & Glasser (2001) showed that this saturation of rheological quantities can also be tied to the saturation of the cluster sizes.

A closer inspection of our data in table 1 reveals that the rate of increase of p and μ with N decreases with the system size. This suggests that there does exist a well-defined thermodynamic limit for the equilibrium rheological properties of a sheared granular system, i.e. they do possess finite limits for $L \to \infty$ and $N \to \infty$

with N/L^2 ($\sim v$) kept constant. However, if the system size is of moderate value ($\tilde{L}/\tilde{d} \sim 50$), the increase in p and μ is only marginal as our work shows. For example, p and μ increase by 1.8% and 1.6%, respectively, when $\tilde{L}/\tilde{d}$ is increased from 39.63 to 112.1 (which is equivalent to an increase of N by a factor of 8). To achieve truly system-independent rheological properties, however, we need to perform simulations with tens of thousands of particles. In order to explore a large parameter space, most of our simulations are restricted to a system with $\tilde{L}/\tilde{d} = 39.63$, and we stress that our results are within about 5% of the asymptotic values for a much larger system.

5. Results: bidisperse system

We consider two different bidisperse systems: (i) a mixture with particles of equal mass, and (ii) a mixture with particles of equal material density. The choice of these two cases was made to clearly delineate the effect of size disparity (case i) from that of size and mass disparities (case ii) on the rheological behaviour of a sheared granular medium. It will become evident that the additional mass disparity for the case (ii) modifies the rheological properties of the mixture in a qualitatively different way.

Typical results are the pressure, the shear viscosity, the granular energy, the ratio of the individual species granular energies, and the first normal stress difference, as functions of the solid fraction, the coefficient of restitution, the size ratio, and the volume fraction ratio. The simulation results are compared with the predictions of the constitutive model (Jenkins & Mancini 1987; Willits & Arnarson 1999) as described in §3.

5.1. *Equal-mass mixture*

In this subsection, the two species are different in size ($R = d_l/d_s > 1$) but we set their masses equal to each other ($m_l = m_s$) in order to isolate the size effects on rheology.

5.1.1. *Solid-fraction dependence of pressure and viscosity*

Figures 4 and 5 show the variations of the pressure and the viscosity with the solid fraction for the size ratio $R = 2$ and the fraction of larger particles $\chi = 0.5$. The values of the coefficients of restitution are $e = 0.99$ in figure 4, and $e = 0.9$ and 0.7 in figure 5. In each plot, the respective partial contributions of each species to pressure and viscosity are also shown. The symbols correspond to the simulation data and the lines to the theoretical predictions as in (3.3) and (3.4).

For the quasi-elastic case ($e = 0.99$), the data for both pressure and viscosity, including their partial components, are in excellent quantitative agreement with the constitutive model up to a solid fraction of $v = 0.5$. As in the monodisperse case, a better choice of the radial distribution function (i.e. replacing v by v/v_{max} in (A 11)) provides good agreement even at $v = 0.6$. For $e = 0.9$, both pressure and viscosity are slightly underpredicted by the constitutive model over the whole range of solid fractions. The partial contributions of the larger species (p_l and μ_l) appear to be better predicted by the model than that of the smaller species. In the case of stronger dissipation ($e = 0.7$), the simulation data are significantly overpredicted by the constitutive model. The model predictions for the partial contributions of the larger species are, again, in somewhat better agreement with simulation data.

5.1.2. *Size-ratio dependence of pressure and viscosity*

In order to quantify the effect of the particle size disparity, we have plotted the variations of the pressure and the viscosity with R in figure 6 at a fixed solid fraction
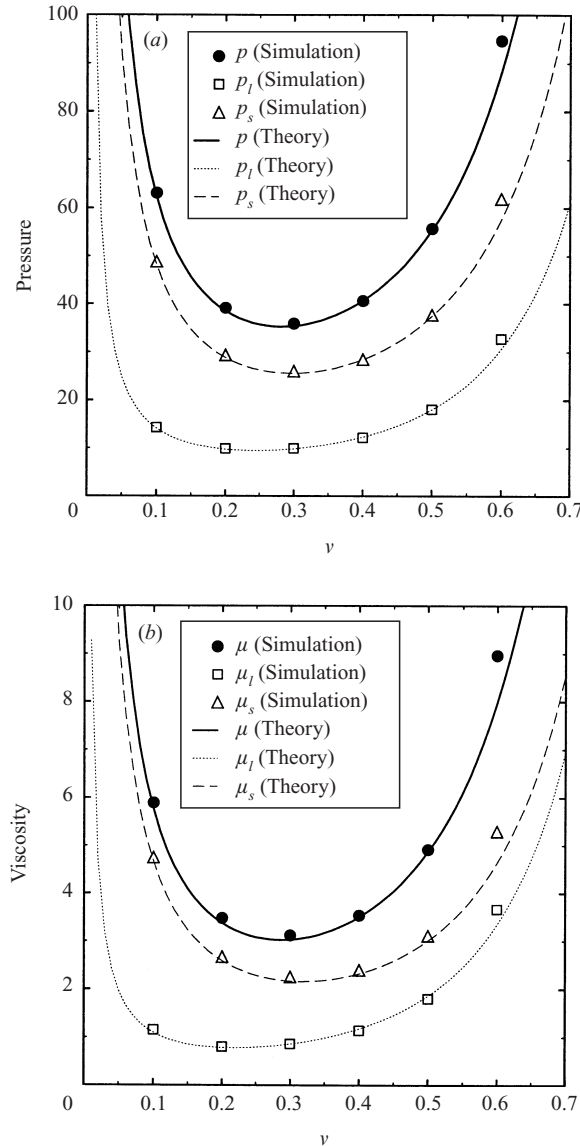
FIGURE 4. Variations of the pressure and the shear viscosity, and their corresponding partial components, with the solid volume fraction for the equal-mass mixture, with $R = 2$, $\chi = 0.5$ and $e = 0.99$.

of $v = 0.3$, with $e = 0.9$ and $\chi = 0.5$. The simulation results for $e = 0.99$ are, again, in excellent agreement with the theory, so that we show neither them nor the results for $e = 0.7$ as they do not lead to new insights. It can be seen from figure 6 that both pressure and viscosity increase with R, and the model predictions are in good qualitative agreement with the simulation data over the whole range of size ratios studied. Note that this behaviour is also in qualitative agreement with our asymptotic scalings for p and μ in the dilute limit as described in §3.2: $p \sim R$ and $\mu \sim R^{3/2}$. The quantitative discrepancy between simulation and theory remains relatively uniform with R, and can be attributed to the fact that the constitutive model is strictly
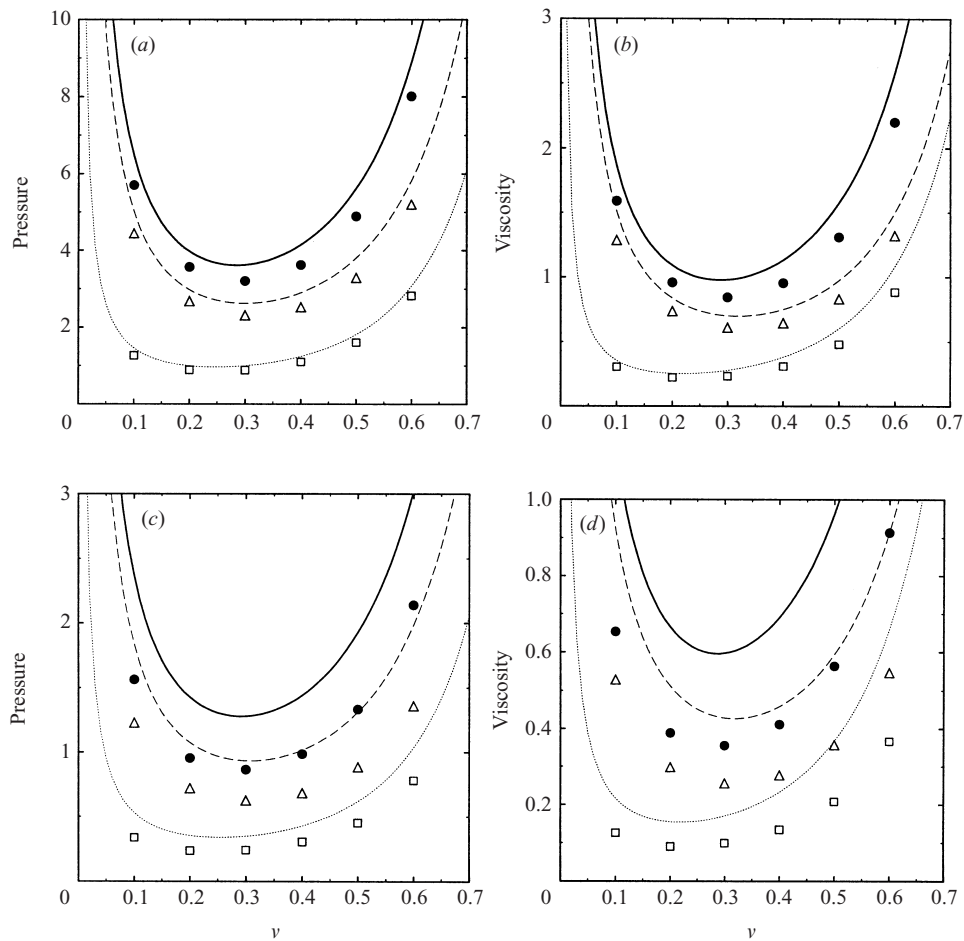
FIGURE 5. As figure 4 but (a,b) $e = 0.9$; (c,d) $e = 0.7$.

valid for the quasi-elastic system, as in the monodisperse case. Regarding the partial components of pressure and viscosity, we note that both p_s and μ_s become more and more dominant with increasing size ratio R. This may be understood by recalling the fact that the number of smaller particles increases with R as $N_s = R^2 N_l \chi_l / \chi_s$ in these simulations (while N_l remains fixed), which in turn increases the magnitudes of p_s and μ_s.

5.1.3. *Mixture granular energy*

In figure 7(a) the variation of the granular energy with the solid fraction, for $R = 2$ and $\chi = 0.5$, is plotted for three different values of the coefficient of restitution. In figure 7(b) the corresponding variation with R is plotted for $\chi = 0.5$, and $v = 0.3$. As in the monodisperse case, the granular energy T decreases with increasing v and decreasing e. The effect of the size disparity is to diminish the value of T further, as can be seen from figure 7(b). Comparing our data with the theoretical predictions, we find that the agreement deteriorates with decreasing e, but the level of disagreement remains uniform up to a size ratio of $R = 5$. The overall comparison for the mixture granular energy between our simulation and theory parallels those for pressure and viscosity, as described in §5.1.1 and §5.1.2.
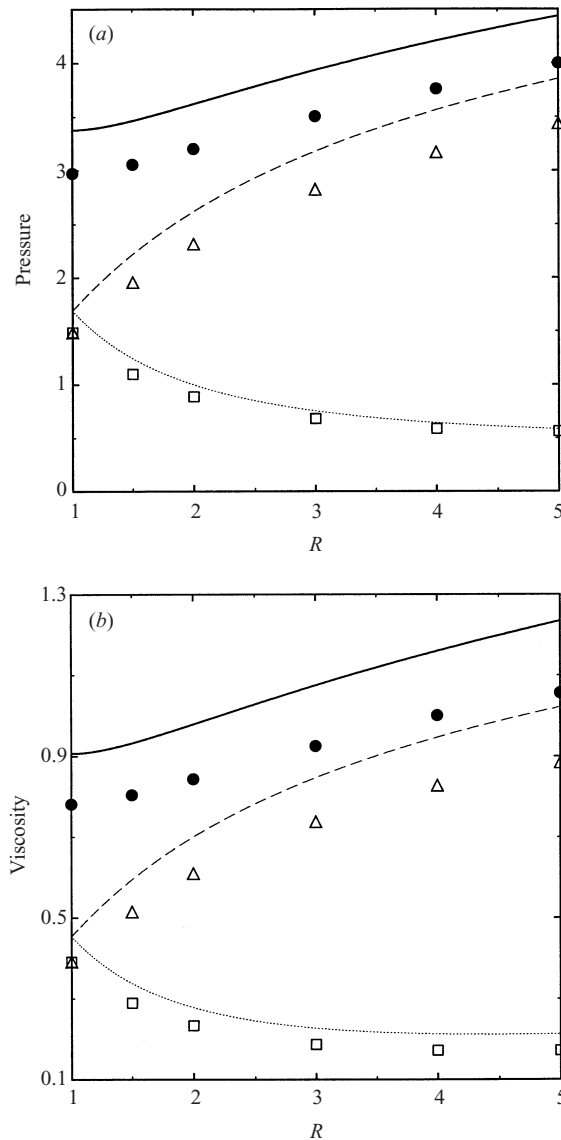
FIGURE 6. Variations of the pressure and the viscosity, and their partial components, with the size-ratio R for an equal mass mixture with $v = 0.3$, $\chi = 0.5$ and $e = 0.9$. Symbols and lines as figure 4.

To find out how the total granular energy is partitioned between the two species, the variation of T_l/T_s with v and R is shown in figures 7(c) and 7(d), for the same simulations as in figures 7(a) and 7(b), respectively. The granular energy is clearly unequally partitioned between the two species, but the level of non-equipartition remains rather small over the range of solid fractions and size ratios studied. Recall that for an equal-mass mixture the granular energy ratio may also be interpreted as the ratio between the squared individual fluctuation velocities, see equation (2.11). Thus, for strong dissipation, the larger particles are somewhat less mobile than the smaller ones, even though both species have the same mass.
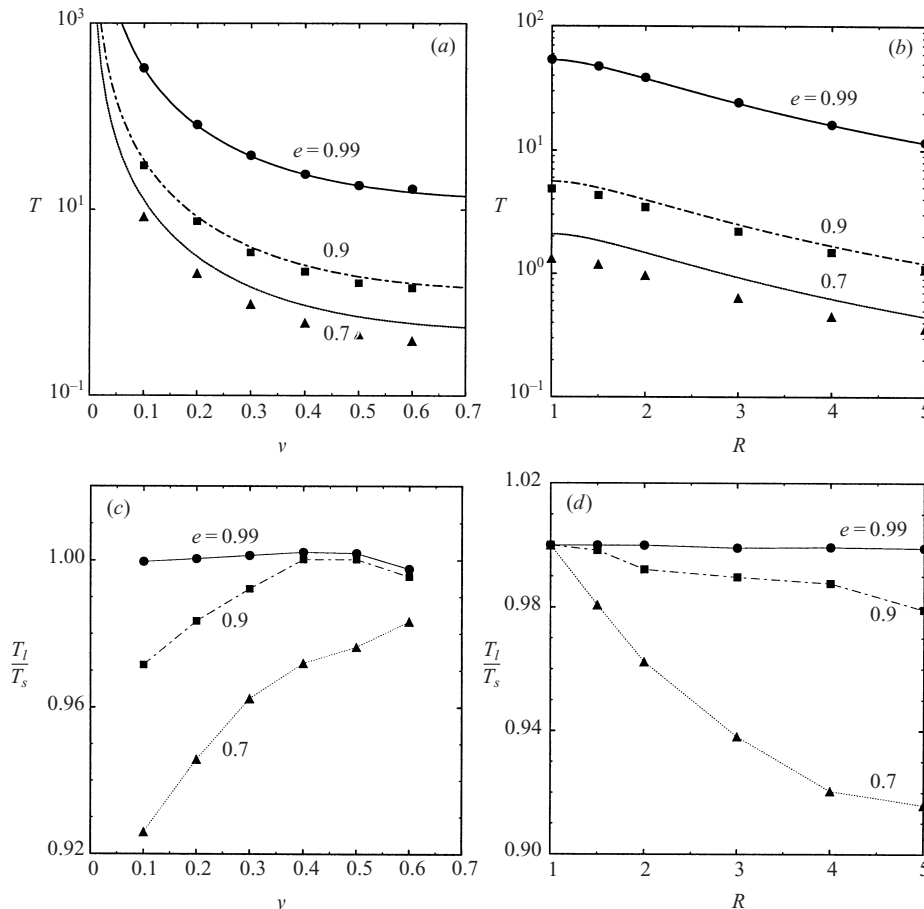
FIGURE 7. Variations of the mixture granular energy T and the ratio of the species granular energies T_l/T_s with the solid volume fraction and the size ratio for an equal-mass mixture. Parameter values are $\chi = 0.5$; (a,c) $R = 2$; (b,d) $v = 0.3$. The lines in (a) and (b) represent the theoretical predictions, whereas the lines in (c) and (d) are drawn to guide the eye.

5.1.4. *Species relative fraction*

Note that all the above results were obtained for mixtures with the same large and small solid fractions, i.e. $\chi = v_l/v = 0.5$. To understand the effect of the relative fraction of larger particles χ on the rheological properties of the fluid, we have plotted the variations of pressure and viscosity with χ in figures 8(a) and 8(b), respectively, for two size ratios $R = 2$ and $R = 5$. The total solid fraction is set to $v = 0.3$ and the coefficient of restitution to $e = 0.9$. It is interesting to note that both pressure and viscosity have peaks at $\chi \approx 2/3$ for $R = 2$, and decrease on either side of the respective peak – the levels of variation in p and μ with χ is about 10%, for $R = 2$. Increasing the size ratio to $R = 5$ increases the height of the peak to a variation of about 50%, with the position of the peak shifted to $\chi \approx 0.85$. Changing the value of the restitution coefficient does not noticeably affect this behaviour.

Again, the theory captures the trend of the data over the whole range of χ studied. The quantitative discrepancies remain relatively uniform with χ. This non-monotonic variation of the shear viscosity with χ suggests that the shear strength of a
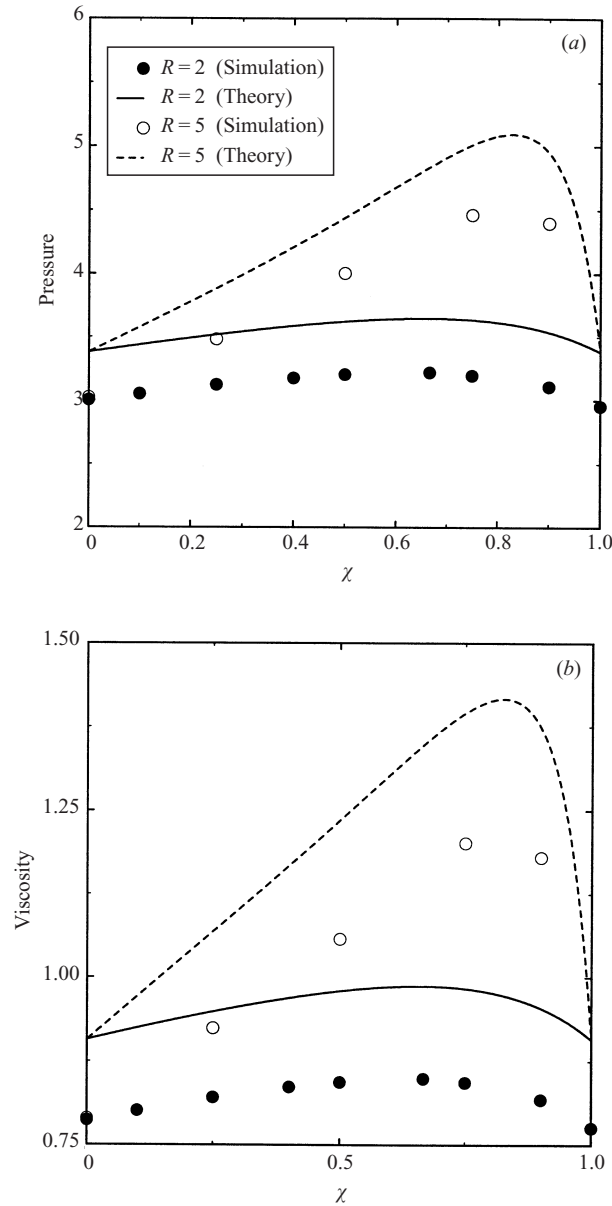
FIGURE 8. The effect of the relative solid volume fraction of the larger species, χ, on (*a*) the pressure and (*b*) the viscosity of an equal-mass mixture, with $v = 0.3$ and $e = 0.9$ for two different size ratios $R = 2$ and $R = 5$.

monodisperse granular fluid can be enhanced by considering an equivalent bidisperse system with particles having the same mass, i.e. adding larger but less dense particles or smaller but denser particles to a monodisperse granular fluid.

5.1.5. *Normal stress difference*

Now we probe the stress anisotropy in an equal-mass mixture. The variation of the first normal stress difference $\mathcal{N}_1$ with solid fraction at a given size ratio is found to be similar to that of the monodisperse system, see figure 3, i.e. $\mathcal{N}_1$ increases in
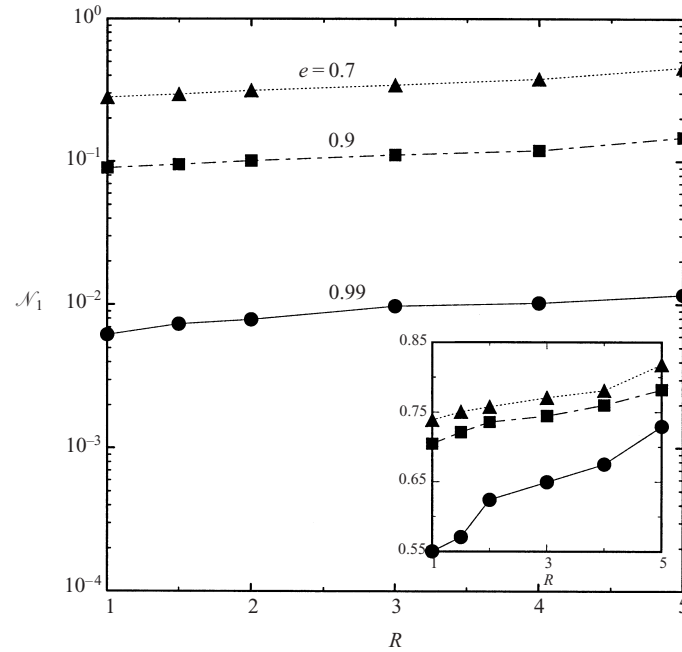
FIGURE 9. Variation of the first normal stress difference $\mathcal{N}_1$ with the size ratio for an equal-mass mixture: $v = 0.3$ and $\chi = 0.5$. The inset shows the variation of $\mathcal{N}_1^k/\mathcal{N}_1$ with R. The symbols denote simulation data and the lines are drawn to guide the eye.

magnitude with decreasing v and e. Thus we restrict our attention only to the effect of the size disparity on the stress anisotropy, i.e. the dependence of $\mathcal{N}_1$ with R, which is shown in figure 9 at a solid fraction $v = 0.3$; the other parameters are as in figure 7(b). It is evident that the size disparity enhances the stress anisotropy, irrespective of the value of the coefficient of restitution. Decomposing $\mathcal{N}_1$ into the respective kinetic and collisional parts ($\mathcal{N}_1 = \mathcal{N}_1^k + \mathcal{N}_1^c$), the relative kinetic contribution $\mathcal{N}_1^k/\mathcal{N}_1$ increases with the size ratio, as can be seen in the inset of figure 9. Thus, the kinetic mode of the momentum transport is primarily responsible for the observed increase in stress anisotropy.

5.1.6. *Large dissipation limit*

As far as the effect of the coefficient of restitution is concerned, the agreement between simulation and theory for the equal-mass bidisperse mixture mirrors that for the monodisperse case. The quantitative agreement worsens with increasing dissipation; however, the qualitative agreement remains reasonable.

Recall that apart from its quasi-elastic assumption, the constitutive model of Willits & Arnarson (1999) further assumes the equality of the two species granular energies which holds approximately for the present case. This suggests that the excellent agreement between theory and simulation for p, μ and T, even at large size ratios, is perhaps not fortuitous. Of course, the model predictions deteriorate on drifting away from the quasi-elastic limit, i.e. when the dissipation is strong, similar to the monodisperse system, as discussed in §4 (see figure 2d). The point to note here is that the level of disagreement remains relatively uniform as the size ratio is increased from the monodisperse limit even at $e = 0.5$ (data not shown here). Thus, the above constitutive model appears to have a wide range of validity in terms of size ratios in

the quasi-elastic limit as long as the mass disparity is of order one. The quantitative disagreement at larger dissipation may be accounted for by developing a higher-order model in terms of the inelasticity.

5.2. *Equal-density mixture*

In this subsection, the particles are again different in size ($R = d_l/d_s > 1$) but now we set their densities equal to each other ($\rho_l = \rho_s$), so that their masses vary quadratically with the size ratio ($m_l/m_s = R^2$). Clearly, this mixture includes the effects of both size and mass disparities, in contrast to the equal-mass mixture which is characterized by its size disparity alone. In presenting the results, we will point out the additional effects of the mass-disparity on the rheological behaviour of such a mixture.

For this case, the variations of pressure and viscosity with solid fraction at a given size ratio (say, $R = 2$) and their comparison with theory mirrors those for the equal-mass mixture, see plots in figure 5. We do not show these results, for the sake of brevity, and directly focus on the effect of the size ratio on the pressure and the viscosity at a fixed solid fraction.

5.2.1. *Size-ratio dependence of pressure and viscosity*

Figure 10 shows the pressure and the viscosity as functions of the size ratio for $v = 0.3$ and $\chi = 0.5$. The values of the coefficients of restitution are $e = 0.99$ for plots (a, b) and $e = 0.9$ for plots (c, d). Note that the insets in plots (c, d) display the quality factor of our data in terms of the ratio between the corresponding simulation and theoretical values. We observe that both pressure and viscosity decrease with increasing size-ratio. This behaviour follows the asymptotic scalings of pressure and viscosity in the dilute limit: $p \sim R^{-1}$ and $\mu \sim R^{-1/2}$ as found in §3.2. For the quasi-elastic case ($e = 0.99$), the theoretical predictions for pressure, viscosity and their partial components agree well with the simulation data even at the largest size ratio of $R = 5$. In the case of larger dissipation ($e = 0.9$), it is observed that even though the theory predicts both p and μ quite well over the whole range of size-ratios (in fact the agreement improves on increasing the size ratio), the partial components of p and μ do not match equally well. For example, both p_l and μ_l are overpredicted by the theory at $R = 1$ but underpredicted at $R = 5$. In contrast, p_s and μ_s are overpredicted over the whole range of size ratios. And this overall trend becomes more prominent when the dissipation level is further increased to $e = 0.7$ (data not shown here).

5.2.2. *Mixture granular energy*

The dependences of the mixture granular energy T on v and R are similar to those for the equal-mass mixture, see figures $7(a)$ and $7(b)$, and hence we do not show these results. The agreement between simulation and theory for T also remains relatively uniform over the range of v and R values studied, as in the equal-mass case.

To illustrate how the total granular energy is partitioned between the two species, we have shown the variation of the ratio of the species granular energies with the solid fraction v and the size ratio R in figures $11(a)$ and $11(b)$, respectively, with the parameter values as in figures $7(c)$ and $7(d)$. From figure $11(a)$, one finds that the granular energy is not equally partitioned between the larger and the smaller species. The magnitude of this non-equipartition increases as the dissipation level increases. This is in contrast to the equal-mass mixture for which we found that the principle of equipartition of granular energy holds approximately for the parameter range studied, see figure $7(c)$. An interesting difference to the equal-mass case is that the degree of non-equipartition increases in the dense limit rather than in the dilute
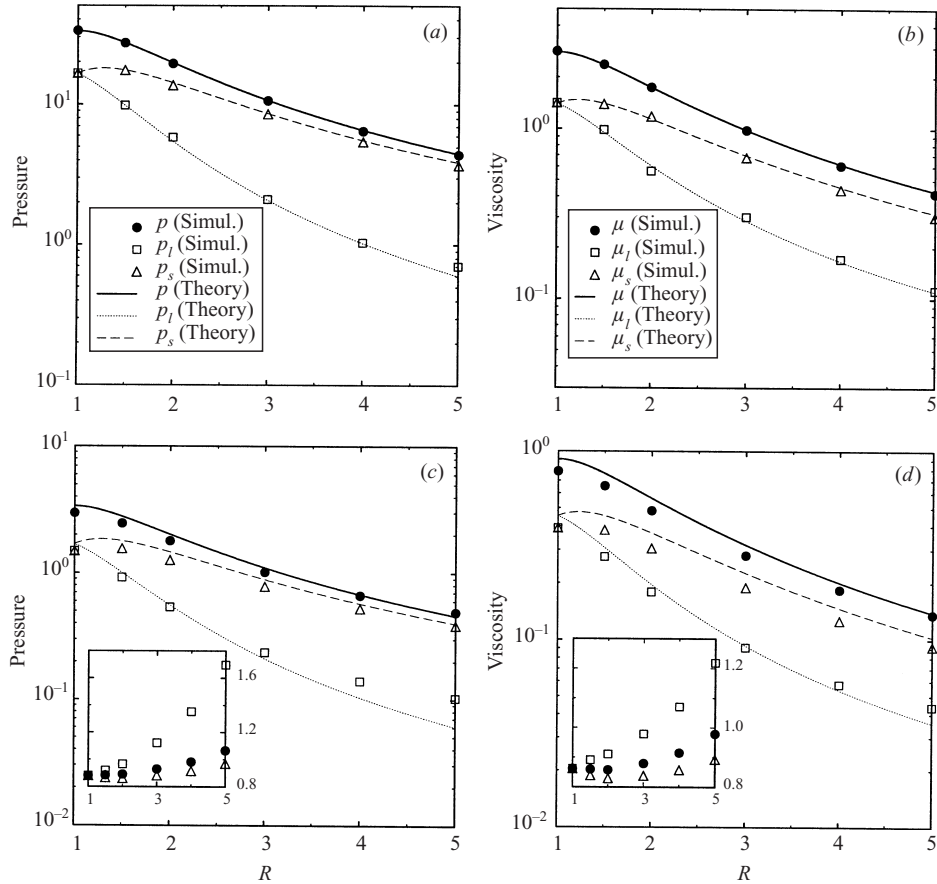
FIGURE 10. Variations of the pressure and the viscosity, and their partial components, with size ratio R for an equal-density mixture with $v = 0.3$, $\chi = 0.5$; (a,b) $e = 0.99$; (c,d) $e = 0.9$. The insets in (c,d) give the respective ratios between the simulation and the theoretical values (e.g. $p_{\text{simu}}/p_{\text{theo}}$).

limit. Examining the effect of the size-ratio, we find that T_l/T_s increases strongly with both R and e. For example, the values of T_l/T_s are 1.4, 4.3 and 12.9 for $e = 0.99$, 0.9 and 0.7, respectively, at a size ratio of $R = 5$.

One can conclude that even though inelasticity is responsible for the onset of energy non-equipartition (as in the equal-mass case), the mass disparity strongly amplifies its magnitude. In the equal-mass case the larger particles have a somewhat smaller granular energy for strong dissipation, whereas in the equal-density case, the larger particles carry the major fraction of the granular energy.

Next, we focus on the 'specific' granular energy, or the granular temperature, defined as $\theta_\alpha = T_\alpha/m_\alpha \equiv \langle C_\alpha C_\alpha/2 \rangle$, a measure for the average fluctuating velocity of the species. The inset in figure 11(a) shows the variation of θ_l/θ_s with v. It is observed that θ_l/θ_s increases with decreasing e, i.e. the larger particles become more mobile, which is in contrast to the equal-mass case for which the increasing dissipation level makes the larger particles relatively less mobile, see figure 7(c).

The effect of the size-ratio on θ_l/θ_s can be seen in the inset in figure 11(b). Here one observes an interesting dichotomy: while the granular temperature ratio decreases monotonically for the quasi-elastic case ($e = 0.99$), its variation is non-monotonic for
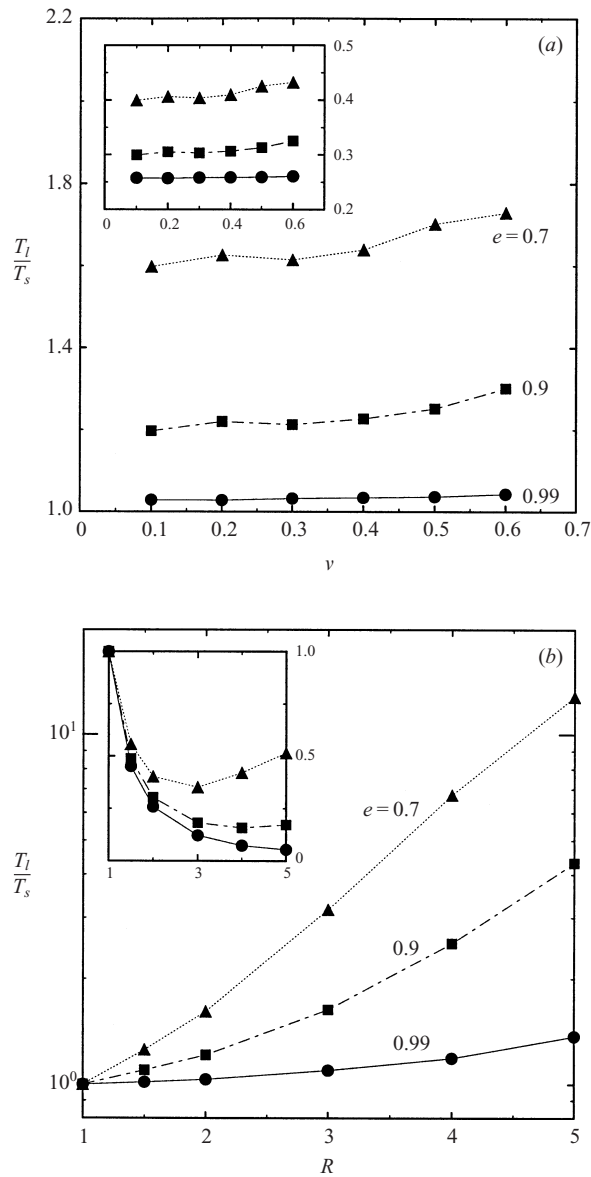
FIGURE 11. Variation of the ratio of the species granular energies T_l/T_s with (*a*) solid volume fraction and (*b*) size ratio for an equal-density mixture: $\chi = 0.5$; (*a*) $R = 2$ and (*b*) $v = 0.3$. The insets give the ratio θ_l/θ_s of the specific granular energies. The lines are drawn to guide the eye.

$e = 0.7$. Further computations suggest that such non-monotonic behaviour prevails even in the quasi-elastic case, if the size-ratio is sufficiently large. Thus, for a given inelasticity, the combined effect of size and mass disparities can lead to a mixture with the fluctuating velocity of the larger particles being of comparable magnitude to that of their smaller counterparts ($\theta_l/\theta_s \sim 1$) if the size ratio is sufficiently large.

5.2.3. *Species relative fraction*

Insights into the effect of the relative fraction of larger particles χ on the rheological properties may be obtained from figure 12, where the variations of pressure and
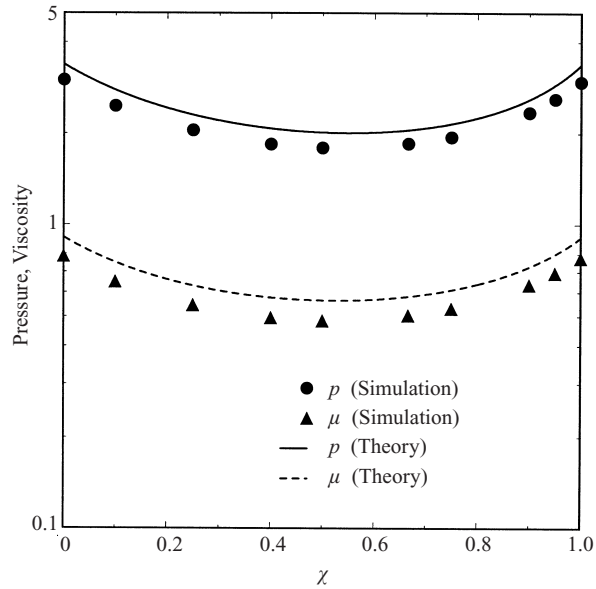
FIGURE 12. The effect of the relative solid volume fraction of the larger species, χ, on the pressure and the viscosity of an equal-density mixture: $v = 0.3$, $R = 2$ and $e = 0.9$.

viscosity with χ are plotted for $v = 0.3$, $R = 2$, and $e = 0.9$. We observe that both pressure and viscosity decrease with increasing χ, reach a minimum at some intermediate value of $\chi \approx 0.6$, and then increase again. Increasing the size ratio lowers the minima considerably: for example, while p and μ decrease by about 30% at a size ratio of $R = 2$, they decrease by about 75% at $R = 5$. Also, the position of this minimum shifts to higher values of χ with increasing size ratio. On the whole, the simulation results agree nicely with the theoretical predictions over the whole range of χ values examined. These results are also in qualitative agreement with the stress measurements of Savage & Sayed (1984) who showed that the shear stresses generated in a monodisperse granular system are about five times higher than those in an equal-density bidisperse mixture with $R = 3.05$ and $\chi = 0.7$. Thus, in contrast to the equal-mass mixture, the mixture becomes less resistant to shearing motion with the addition of a small amount of another species of the same material density.

The variation of the ratio of the species granular energies (T_l/T_s) with χ is plotted in figure 13 for the same parameter values as in figure 12. We observe that even though the maximum non-equipartition of energy ($T_l/T_s)_{max}$ is attained at some intermediate value of $\chi \approx 0.5$, the degree of non-equipartition remains relatively uniform with varying χ.

5.2.4. *Normal stress difference*

Turning our attention to the stress anisotropy, we show the variation of the first normal stress difference, $\mathcal{N}_1$, with R in figure 14, for $v = 0.3$ and $\chi = 0.5$. One can observe that even though the variations of $\mathcal{N}_1$ with R are similar to that of the equal-mass mixture, see figure 9, the magnitude of $\mathcal{N}_1$ for the equal-density case is slightly larger than that for the equal-mass mixture, irrespective of the value of the coefficient of restitution. For example, the value of $\mathcal{N}_1$ increases by 11.2% and 25.3% at size ratios of $R = 2$ and $R = 5$, respectively, for $e = 0.9$. In the inset of figure 14,
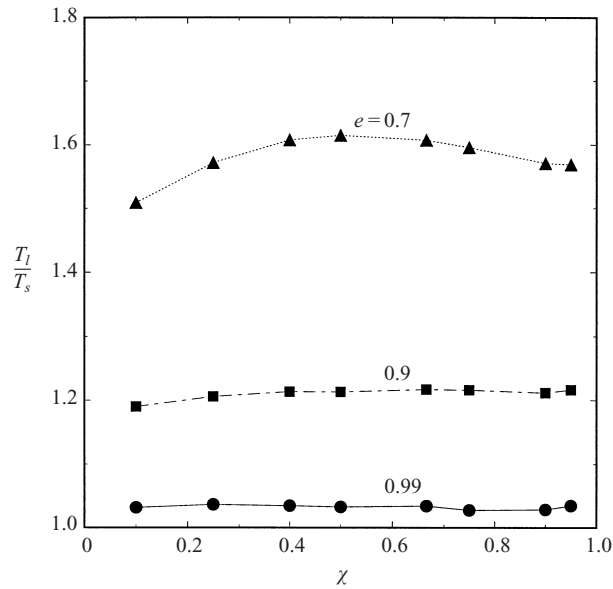
FIGURE 13. The effect of the relative solid volume fraction of the larger species, χ, on the granular energy ratio of an equal-density mixture: $v = 0.3$ and $R = 2$. The lines are drawn to guide the eye.
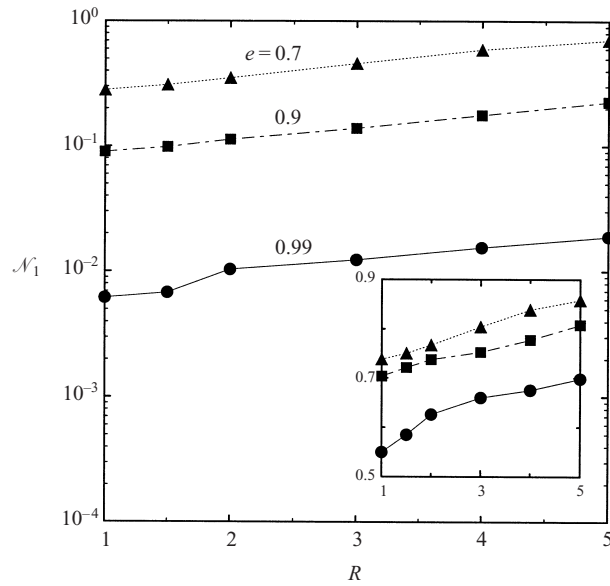

FIGURE 14. Variation of the first normal stress difference $\mathcal{N}_1$ with the size ratio for an equal-density mixture: $v = 0.3$ and $\chi = 0.5$. The inset shows the variation of the kinetic fraction $\mathcal{N}_1^k/\mathcal{N}_1$ with R. The lines are drawn to guide the eye.

the kinetic fraction to the normal stress difference, $\mathcal{N}_1^k/\mathcal{N}_1$ is shown. It increases with R, which confirms that the kinetic mode of stress transmission is mainly responsible for the enhanced stress anisotropy with increasing size ratio. Finally, we mention that the first normal stress difference does not change much with χ if the overall solid fraction is held constant.

6. Discussion: non-equipartition of granular energy

In §6.1 we make a qualitative comparison of our data on the granular energy ratio with recent experimental measurements and also with a theoretical model. In §6.2 we discuss the effect of large mass disparities and the associated energy non-equipartition on the rheological properties of the mixture.

6.1. *Comparison with experiment and theory*

The microgravity experiments of Louge *et al.* (2001) on collisional shear flows of binary mixtures are most appropriate for direct comparison to the present work. Even though these experiments did show signatures of energy non-equipartition (see their figure 4), the evidence was not conclusive due to the limited amount of data, and also due to the small size disparity ($R = 1.25$ and hence small mass-disparity) and the quasi-elastic ($e = 0.93$) nature of their granular mixture.

However, the recent experiments of Feitosa & Menon (2002) clearly make a case for the breakdown of energy equipartition. They have done a series of careful experiments, measuring the fluctuating kinetic energies of each species of a mixture of equal-size particles vibrated in a two-dimensional cell. For a mixture of glass and aluminium particles of almost equal mass ratio ($m_{alu}/m_{glass} = 1.1$), they found that the granular energy is equally partitioned between the two species within the experimental errors. But for mixtures of steel–glass or brass–glass particles (with mass ratios $m_{steel}/m_{glass} = 3$ and $m_{brass}/m_{glass} = 3.4$), they found that the heavier particles could carry as much as 50% more energy compared to the lighter particles ($T_{heavy}/T_{light} \approx 1.5$). The effect of gravity on their reported results can be neglected since the energy ratio did not vary noticeably on increasing the Froude number ($Fr = U_o^2/gd_l$, where U_o is the velocity of the vibrating plate) from 50 to 130. Hence the non-equipartition of energy is a bulk effect, solely determined by the detailed balance between the injected energy through the bottom-plate vibration and the collisional dissipation.

Our simulation data for an equal-size particle mixture with a mass ratio of 3 show that $T_{heavy}/T_{light} = 1.08$, 1.63 and 2.05 for the coefficients of restitution of $e = 0.99$, 0.9 and 0.8, respectively. Note that Feitosa & Menon measured only the effective inelasticity for the single-component systems which translates into the value of e being in the range between 0.78 and 0.91. Also recalling the fact that our simulations were performed using a single value for $e \equiv e_{\alpha\beta}$, the agreement between simulation and experiment can be said to be fair. Two other observations of these experiments, namely that the energy ratio depends only weakly on both the average solid fraction and the number fraction, are also in qualitative agreement with our simulations (see figures 11*a* and 14).

Turning our attention now to the possible theoretical description of energy non-equipartition, we consider the recent work of Garzó & Dufty (1999) who studied the homogeneous cooling state for a binary granular mixture using the Enskog kinetic theory. They showed that the granular energies of each species are different, even though their cooling rates are the same. They derived a functional relation for the ratio of the species granular energies which, in the quasi-elastic limit, simplifies to

$$
\frac{T_l}{T_s} = 1 + \left(\frac{\xi_l}{M_{sl}} - \frac{\xi_s}{M_{ls}} \right) \frac{(1-e_{ls})}{2} + \frac{\xi_s}{M_{ls}} \frac{g_{ss}}{g_{ls}} \left(\frac{2}{1+R_{ls}} \right)^{d-1} \sqrt{\frac{M_{ls}}{2M_{sl}^2}} \frac{(1-e_{ss})}{2}
$$

$$
- \frac{\xi_l}{M_{sl}} \frac{g_{ll}}{g_{sl}} \left(\frac{2}{1+R_{sl}} \right)^{d-1} \sqrt{\frac{M_{sl}}{2M_{ls}^2}} \frac{(1-e_{ll})}{2}, \quad (6.1)
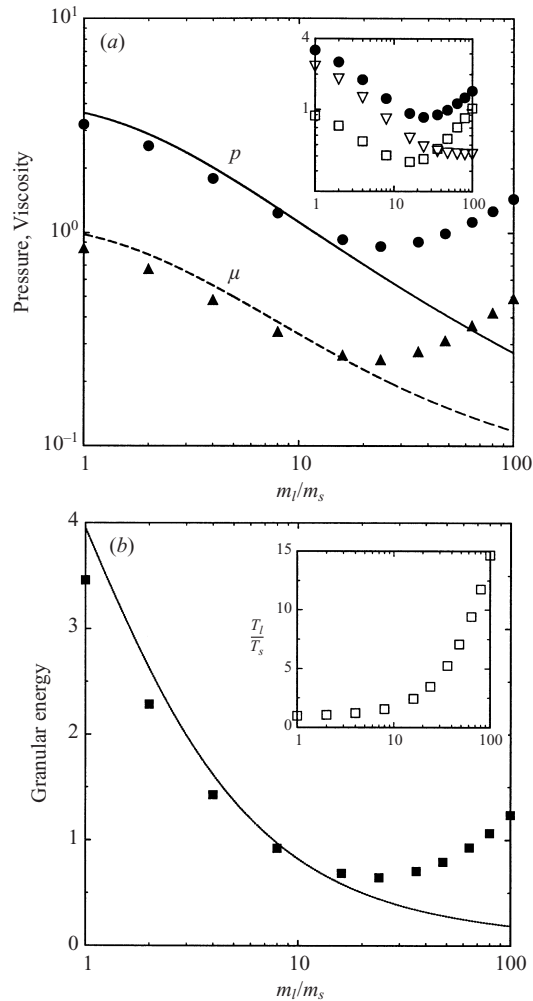$$

FIGURE 15. The effect of mass ratio, m_l/m_s, on (a) the pressure and viscosity (b) the granular energy: $v = 0.3$, $R = 2$, $\chi = 0.5$ and $e = 0.9$. The inset in (a) shows variations of p, p_l ($\square$) and p_s (∇), and the inset in (b) shows the variation of T_l/T_s.

where d is the dimensionality of the system. It can be readily verified from (6.1) that inelasticity alone leads to the non-equipartition of energy, and the added mass disparity just enhances its magnitude. Comparing our results for $e = 0.99$ with equation (6.1), we find that the theory underpredicts the simulation results by about 2.5% and 33% at $R = 2$ and 5, respectively, for an equal-density mixture, but the agreement with the equal-mass case is within 1% for both size ratios.

On the whole, our simulation results are in good agreement with the experiments of Feitosa & Menon (2002), but the agreement with the theoretical predictions of Garzo & Dufty (1999) is only qualitative. We can conclude from these comparisons that the breakdown of energy equipartition in a granular mixture is a generic phenomenon and occurs due to the micro-scale dissipation associated with the inelastic nature of the particle collisions.

6.2. *Effect on rheological properties*

The effect of large mass disparities on the pressure and viscosity is shown in figure 15(*a*), with parameter values $v = 0.3$, $R = 2$, $\chi = 0.5$ and $e = 0.9$. (Note that since the size ratio is kept fixed, the species number densities are also fixed for this figure.) We observe that both pressure and viscosity show interesting non-monotonic behaviour with the mass ratio. In contrast, however, the theoretical predictions suggest monotonic decay in the same limit. The corresponding comparison between simulation and theory for the granular energy, in figure 15(*b*), shows similar behaviour. On decreasing the coefficient of restitution, all the above quantities show non-monotonic behaviour at lower values of the mass ratio. Looking at the variations of the partial pressures in the inset of figure 15(*a*) (the corresponding variations for partial viscosities are similar and, hence, not shown in this graph), we find that at large mass disparities the major contribution to pressure (and viscosity) comes from the heavier particles only. This is primarily due to the strong non-equipartition of granular energy at large mass disparities, as seen in the inset of figure 15(*b*). The relative contributions of the two species can be understood by postulating a simple constitutive relation for the pressure:

$$p = \sum_{\alpha=l,s} p_\alpha = \sum_{\alpha=l,s} f_{1\alpha} T_\alpha. \tag{6.2}$$

Recall that the variations of both p and μ with solid fraction follow U-shaped curves, with minima occurring at $v \approx 0.3$ (see figures 2*a* and 2*b*). Since the relative contribution of the heavier particles to transport properties is large due to their higher granular energy at large mass-ratios, the mixture would behave as if it were composed of only heavier particles with an effective lower solid fraction, depending on the relative solid fraction of heavier species χ. Hence both pressure and viscosity would eventually increase in the same limit. A phenomenological constitutive model has recently been suggested (Alam & Luding 2002*a*), allowing non-equipartition of granular energy, which could explain the non-monotonic behavior of p, μ and T with the mass ratio.

7. Summary and conclusion

We have carried out event-driven simulations in two dimensions for bidisperse granular mixtures undergoing uniform shear flow, with the goal of understanding the effect of bidispersity on the rheology of such mixtures. The Lees–Edwards boundary condition was used to attain the state of uniform shear, and the granular mixture was modelled as smooth, inelastic hard disks, where the two species differ in size and mass. In order to distinguish between the effects of size and mass disparities, equal-mass and equal-density mixtures, were considered. Results on the pressure, shear viscosity, granular energy and first normal stress difference were reported in a wide parameter space. The simulation results were compared with a kinetic-theory constitutive model (Willits & Arnarson 1999; Alam *et al.* 2002). Qualitative comparisons of some of the simulation results were also made with some experiments (Savage & Sayed 1984; Feitosa & Menon 2002), and with another theoretical model (Garzó & Dufty 1999) which takes into account the non-equipartition of granular energy.

For the briefly revisited monodisperse system, it is shown that even though both pressure and viscosity depend on the size of the system (i.e. on the number of the particles), there appears to exist a thermodynamic limit for these quantities. Thus, the

equilibrium rheological properties can reliably be obtained by simulating a system of moderate size (of the order of a few thousand particles). The assumption of the homogeneity of the system was not discussed in detail; however, we checked that the data presented stem from almost homogeneous systems.

For bidisperse mixtures, we have found that both the pressure and the viscosity increase or decrease with increasing size ratio, depending on whether the particles are of the same mass or density, respectively. In other words, the mixture becomes more/less resistant to the shearing motion with the addition of a small amount of another species of the same mass/density, compared to its equivalent monodisperse counterpart. The maximum increase/decrease in pressure and viscosity that can be achieved for a given mixture depends crucially on both the size ratio and the relative fraction of the two species. For a larger size disparity, fewer particles of the smaller species are needed to achieve a maximum increase/decrease in the shear strength of the mixture. Regarding the granular energy, we have found that it is unequally partitioned between the two species (as in earlier studies) and the onset of this non-equipartition is clearly linked to the inelasticity of the particle collisions. The level of energy non-equipartition increases with increasing dissipation strength and with increasing size and mass disparities. It is the mass disparity between the two species that significantly increases the level of energy non-equipartition.

Regarding the comparisons with the constitutive model, we have shown that the agreement between simulation and theory for pressure, viscosity and granular energy is excellent even at a size ratio of 5 for both types of mixtures as long as the coefficient of restitution remains close to unity ($e = 0.99$). This can be attributed to the fact that the principle of equipartition of granular energy holds approximately in this limit for the parameter range investigated. As the coefficient of restitution is decreased, all the above quantities are overpredicted over the whole range of size ratios for the equal-mass mixture, similar to the monodisperse case. For the equal-density case, on the other hand, the theoretical predictions for the partial components of the pressure and the viscosity worsen considerably with increasing dissipation level, even though the total pressure and viscosity are relatively well predicted in the studied parameter range. For a given size ratio, both pressure and viscosity show interesting non-monotonic variation with the mass ratio (depending on the relative solid fraction of the heavier particles), while the theoretical predictions suggest monotonic decay in the same limit.

In general, the granular fluid is non-Newtonian in that the stress tensor is anisotropic, giving rise to 'measurable' normal stress differences. We have found that the effect of size dispersity is to increase the magnitude of the first normal stress difference, thus enhancing the non-Newtonian character of the fluid, and the added mass disparity in the equal-density mixture further increases its magnitude. For both cases, however, it is the kinetic-mode of momentum transport which is primarily responsible for this enhanced normal stress difference.

The results of this study suggest several possibilities for future investigations. On the theoretical side, a constitutive model taking into account the non-equipartition of granular energy is required for all practical occurrences of large mass disparity and strong dissipation. In this regard, the constitutive model of Jenkins & Mancini (1987) can be appropriately modified to obtain a minimal model with energy non-equipartition (Alam & Luding 2002*a*). At the next level, it is also necessary to incorporate the stress anisotropy in such a model, perhaps following the earlier work of Jenkins & Richman (1988) on monodisperse systems. We should, however, point out that such a rigorous theory for a bidisperse system would be too complicated to

be useful as a practical tool. As an alternative one could also consider relaxation-type models for the stress tensor (Goddard 1977, 1984; Jin & Slemrod 2001), with the relaxation time being a free-parameter which may be obtained from simulation data. Although less rigorous, such an approach holds promise for predictive and practical purposes. On the simulation side, as a direct extension of the present work we are now looking at the dense limit, focusing on the subtle roles of inelasticity and bidispersity on the glassy dynamics of a sheared system (Alam & Luding 2002*b*). Future work should also investigate the effects of the tangential coefficient of restitution, the Coulomb friction and the bounding wall on the bulk rheology of the mixture.

Appendix. Balance laws and the constitutive model

We consider a mixture of two types of particles, labelled l and s, with diameters $\tilde{d}_\alpha$ ($\alpha = l, s$), species masses $\tilde{m}_\alpha$, species densities $\tilde{\varrho}_\alpha = \tilde{m}_\alpha \tilde{n}_\alpha$, and species number density $\tilde{n}_\alpha$. The species densities are related to the volume fraction v_α and the material density $\tilde{\rho}_\alpha$ via the relation $\tilde{\varrho}_\alpha = v_\alpha \tilde{\rho}_\alpha$. The relevant hydrodynamic fields, at the level of mixture theory, are the species number density $\tilde{n}_\alpha$, the mixture ('hydrodynamic') velocity $\tilde{\boldsymbol{u}} = \sum_{\alpha = l, s} \tilde{\varrho}_\alpha \tilde{\boldsymbol{u}}_\alpha / \tilde{\varrho}$, and the mixture granular energy.

In the absence of any external force, the balance equations for number density, momemtum and granular energy may be written as (in dimensional form) (Lopez de Haro, Cohen & Kincaid 1983; Jenkins & Mancini 1987, 1989; Willits & Arnarson 1999)

$$\frac{\mathrm{D}\tilde{n}_\alpha}{\mathrm{D}\tilde{t}} = -\tilde{n}_\alpha \tilde{\boldsymbol{\nabla}} \cdot \tilde{\boldsymbol{u}} - \tilde{\boldsymbol{\nabla}} \cdot \tilde{\boldsymbol{j}}_\alpha, \tag{A 1}$$

$$\tilde{\varrho} \frac{\mathrm{D}\tilde{\boldsymbol{u}}}{\mathrm{D}\tilde{t}} = -\tilde{\boldsymbol{\nabla}} \cdot \tilde{\boldsymbol{P}}, \tag{A 2}$$

$$\tilde{n} \frac{\mathrm{D}\tilde{T}}{\mathrm{D}\tilde{t}} = \tilde{T} \tilde{\boldsymbol{\nabla}} \cdot \tilde{\boldsymbol{j}} - \tilde{\boldsymbol{\nabla}} \cdot \tilde{\boldsymbol{q}} - \tilde{\boldsymbol{P}} : \tilde{\boldsymbol{\nabla}} \tilde{\boldsymbol{u}} - \tilde{\mathscr{D}}, \tag{A 3}$$

where $\tilde{\varrho} = \sum_\alpha \tilde{m}_\alpha \tilde{n}_\alpha$ is the mixture mass density, $\tilde{\boldsymbol{P}} = \sum_\alpha \tilde{\boldsymbol{P}}_\alpha$ the total stress tensor (defined in the compressive sense), $\tilde{\boldsymbol{j}} = \sum_\alpha \tilde{\boldsymbol{j}}_\alpha = \sum_\alpha \tilde{n}_\alpha \tilde{\boldsymbol{v}}_\alpha^d$ the particle flux associated with diffusion velocities, $\tilde{\boldsymbol{q}}$ the mixture flux of granular energy, and $\tilde{\mathscr{D}}$ the rate of dissipation of granular energy per unit volume. The species diffusion velocity $\tilde{\boldsymbol{v}}_\alpha^d = \tilde{\boldsymbol{u}}_\alpha - \tilde{\boldsymbol{u}}$ is defined as the difference between the average species velocity $\tilde{\boldsymbol{u}}_\alpha$ and the mixture velocity $\tilde{\boldsymbol{u}}$.

The constitutive relations for the stress tensor and the collisional dissipation are (Jenkins & Mancini 1987; Willits & Arnarson 1999)

$$\tilde{\boldsymbol{P}} = \tilde{p}\boldsymbol{1} - 2\tilde{\mu}\tilde{\boldsymbol{S}} - \tilde{\lambda}(\tilde{\boldsymbol{\nabla}} \cdot \tilde{\boldsymbol{u}})\boldsymbol{1}, \tag{A 4}$$

$$\tilde{p} = \frac{4}{\pi}\tilde{d}_l^{-2}\tilde{T}\sum_{\alpha = l, s} f_{1\alpha}, \tag{A 5}$$

$$\tilde{\mu} = \sqrt{\tilde{\rho}_l \tilde{T}} \sum_{\alpha=l,s} f_{2\alpha} \sqrt{\frac{\rho_\alpha}{\rho_l}}, \tag{A 6}$$

$$\mathscr{D} = \frac{\sqrt{\tilde{\rho}_l}}{\tilde{m}_l \tilde{d}_l^2} \tilde{T}^{3/2} \sum_{\alpha=l,s} f_{5\alpha} R_{l\alpha}^2 \frac{m_l}{m_\alpha} \sqrt{\frac{\rho_\alpha}{\rho_l}}. \tag{A 7}$$

The non-dimensional functions, f_1, f_2 and f_5, in the expressions for pressure, shear viscosity and collisional dissipation are

$$f_{1\alpha} = v_\alpha R_{l\alpha}^2 \left(1 + \tfrac{1}{4}\sum_{\beta=l,s}(1+e_{\alpha\beta})(1+R_{\alpha\beta})^2 v_\beta g_{\alpha\beta}\right), \tag{A 8}$$

$$f_{2\alpha} = \frac{\overline{b}_{\alpha 0}}{2} + \frac{1}{4}\sum_{\beta=l,s} v_\beta g_{\alpha\beta} M_{\beta\alpha}(1+R_{\alpha\beta})^2 \left(\overline{b}_{\alpha 0} + \frac{v_\alpha R_{\beta\alpha}(1+R_{\alpha\beta})}{\sqrt{\pi^2 M_{\beta\alpha}/2}}\right), \tag{A 9}$$

$$f_{5\alpha} = \frac{4v_\alpha}{\pi}\sum_{\beta=l,s} v_\beta(1+R_{\beta\alpha})R_{\alpha\beta}^2 g_{\alpha\beta}(1-e_{\alpha\beta}^2)\sqrt{2M_{\beta\alpha}}, \tag{A 10}$$

where

$$\overline{b}_{\alpha 0} = \frac{\sqrt{M_{\kappa\alpha}}}{\sqrt{2}(1+R_{\kappa\alpha})g_{\alpha\kappa}}\left[\frac{(v_\alpha/v_\kappa)R_{\kappa\alpha}^2 K_\alpha' B_\alpha + K_\kappa' M_{\alpha\kappa} M_{\kappa\alpha}}{B_\alpha B_\kappa - M_{\alpha\kappa}^2 M_{\kappa\alpha}^2}\right],$$

$$B_\alpha = M_{\alpha\kappa}(1+M_{\kappa\alpha}) + \frac{R_{\alpha\kappa}^2}{(1+R_{\alpha\kappa})}\frac{v_\kappa}{v_\alpha}\frac{g_{\kappa\kappa}}{g_{\alpha\kappa}}\left(\frac{M_{\alpha\kappa}}{M_{\kappa\kappa}}\right)^{1/2},$$

$$K_\alpha' = 1 + \frac{1}{2}\sum_{\beta=l,s} v_\beta(1+R_{\alpha\beta})^2 g_{\alpha\beta} M_{\beta\alpha},$$

with $\alpha \neq \kappa$. Note that the factor $(M_{\alpha\kappa}/M_{\kappa\kappa})^{1/2}$ in the second term of B_α is missing from the corresponding expression of Willits & Arnarson (1999), as subsequently rectified (Alam *et al.* 2002). The radial distribution function at contact $g_{\alpha\beta}$ is (Mansoori *et al.* 1971)

$$g_{\alpha\beta} = \frac{1}{(1-v)} + \frac{9}{8}\frac{(v_l R_{\alpha l} + v_s R_{\alpha s})}{(1+R_{\alpha\beta})(1-v)^2}, \tag{A 11}$$

with $R_{ss} = R_{ll} = 1$ and $R_{ls} = R_{sl}^{-1} = R$. We should point out that $g_{\alpha\beta}$ should diverge at the close packing limit ($v = v_{max}$), rather than at $v \to 1$. This corresponds to $v_{max} \approx 0.9069$ for a perfectly monodisperse system; for a bidisperse system, v_{max} is also a function of the size ratio (Luding & Strauß 2001). However, we performed simulations up to an overall solid fraction of 0.6, which is well below the freezing point density, and we have checked that the theoretical predictions for pressure and viscosity are independent of the choice of a more correct radial distribution function for $v \leqslant 0.55$.

REFERENCES

ALAM, M. & LUDING, S. 2002*a* How good is the equipartition assumption for the transport properties of a granular mixture? *Gran. Matt.* **4** (in press).
ALAM, M. & LUDING, S. 2002*b* First normal stress difference and crystallization in a dense sheared granular fluid. *Phys. Fluids* (submitted).
ALAM, M., WILLITS, J. T., ARNARSON, B. Ö. & LUDING, S. 2002 Kinetic theory of a binary mixture of nearly elastic disks with size and mass disparity. *Phys. Fluids* (in press).
ALLEN, M. P. & TILDESLEY, D. J. 1989 *Computer Simulations of Liquids.* Clarendon.

ARNARSON, B. Ö. & WILLITS, J. T. 1998 Thermal diffusion in binary mixtures of smooth, nearly elastic spheres with and without diffusion. *Phys. Fluids* **10**, 1324–1328.

BEHRINGER, R. P. & JENKINS, J. T. 1997 *Powders & Grains*. Balkema.

CAMPBELL, C. S. 1989 The stress tensor for simple shear flows of a granular material. *J. Fluid Mech.* **203**, 449–473.

CAMPBELL, C. S. 1990 Rapid granular flows. *Annu. Rev. Fluid Mech.* **22**, 57–91.

CHOWHAN, Z. T. 1995 Segregation of particulate solids: Part I. *Pharm. Tech.* **19**, 56–63.

ERPENBECK, J. J. & WOOD, W. W. 1981 Molecular dynamics calculations of shear viscosity time-correlation functions for hard spheres. *J. Statist. Phys.* **24**, 455.

FEITOSA, K. & MENON, N. 2002 Breakdown of energy nonequipartition in a 2D binary vibrated gas. *Phys. Rev. Lett.* **88**, 198301-1.

FERZIGER, J. H. & KAPER, H. G. 1972 *Mathematical Theory of Transport Processes in Gases*. North-Holland.

FOSS, D. R. & BRADY, J. F. 2000 Structure, diffusion and rheology of Brownian suspensions by Stokesian Dynamics simulation. *J. Fluid Mech.* **407**, 167–200.

GARZO, V. & DUFTY, J. 1999 Homogeneous cooling state for a granular mixture. *Phys. Rev. E* **60**, 5706–5713.

GODDARD, J. D. 1977 Polymer fluid mechanics. *Adv. App. Mech.* **19**, 143–197.

GODDARD, J. D. 1984 Dissipative materials as models of thixotropy and plasticity. *J. Non-Newtonian Fluid Mech.* **14**, 141–157.

GOLDSHTEIN, A. & SHAPIRO, M. 1995 Mechanics of collisional motion of granular materials. Part 1. General hydrodynamic equations. *J. Fluid Mech.* **282**, 75–114.

HAFF, P. K. 1983 Grain flow as a fluid mechanical phenomenon. *J. Fluid Mech.* **134**, 401–430.

HERRMANN, H. J., HOVI, J.-P. & LUDING, S. 1998 *Physics of Dry Granular Media*. Kluwer Academic, Holland.

HONG, D. C., QUINN, P. V. & LUDING, S. 2001 The reverse Brazil nut problem: Competition between percolation and condensation. *Phys. Rev. Lett.* **86**, 3423–3426.

HOPKINS, M. A. & LOUGE, M. Y. 1991 Inelastic microstructure in rapid granular flows of smooth disks. *Phys. Fluids* A **3**, 47–59.

JENKINS, J. T. & MANCINI, F. 1987 Balance laws and constitutive relations for plane flows of a dense, binary mixture of smooth, nearly elastic, circular disks. *Trans. ASME: J. Appl. Mech.* **54**, 27–34.

JENKINS, J. T. & MANCINI, F. 1989 Kinetic theory for binary mixtures of smooth, nearly elastic spheres. *Phys. Fluids* A **1**, 2050–2059.

JENKINS, J. T. & RICHMAN, M. W. 1985 Kinetic theory for plane shear flows of a dense gas of identical, rough, inelastic, circular disks. *Phys. Fluids* **28**, 3485–3499.

JENKINS, J. T. & RICHMAN, M. W. 1988 Plane simple shear of smooth inelastic circular disks: the anisotropy of the second moment in the dilute and dense limits. *J. Fluid Mech.* **192**, 313–329.

JENKINS, J. T. & SAVAGE, S. 1983 A theory for the rapid flow of identical, smooth, nearly elastic, spherical particles. *J. Fluid Mech.* **130**, 187–202.

JIN, S. & SLEMROD, M. 2001 Regularization of the Burnett equations for rapid granular flows via relaxation. *Physica* D **150**, 207–225.

KISHINO, Y. 2001 *Powders & Grains*. Balkema.

LÄTZEL, M., LUDING, S. & HERRMANN, H. J. 2000 Macroscopic material properties from quasistatic, microscopic simulations of a two-dimensional shear-cell. *Gran. Matt.* **2**, 123–135.

LEES, A. W. & EDWARDS, S. F. 1972 The computer study of transport processes under extreme conditions. *J. Phys. C* **5**, 1921.

LISS, E. D. & GLASSER, B. J. 2001 The influence of clusters on the stress in a sheared granular material. *Powder Tech.* **116**, 116.

LOPEZ DE HARO, M., COHEN, E. G. D. & KINCAID, J. M. 1983 The Enskog theory for multicomponent mixtures. I. Linear transport theory. *J. Chem. Phys.* **78**, 2746.

LOUGE, M. Y. 1994 Computer simulations of rapid granular flows of spheres interacting with a flat, frictional boundary. *Phys. Fluids* A **6**, 2253–2269.

LOUGE, M. Y., JENKINS, J. T., XU, H. & ARNARSON, B. Ö. 2001 Granular segregation in collisional shearing flows. In *Mechanics for a New Millenium* (ed. H. Aref & J. W. Phillips), pp. 239–252. Kluwer.

Luding, S. 2001 Global equation of state for two-dimensional hard sphere system. *Phys. Rev.* E **63**, 042201-1.

Luding, S., Huthmann, M., McNamara, S. & Zippelius, A. 1998 Homogeneous cooling of rough dissipative particles: Theory and simulations. *Phys. Rev.* E **58**, 3416–3425.

Luding, S. & Herrmann, H. J. 1999 Cluster growth in freely cooling granular media. *Chaos* **9**, 673–681.

Luding, S. & Strauss, S. 2001 The equation of state for polydisperse granular gases. In *Granular Gases* (ed. T. Pöschel & S. Luding), pp. 389–409. Springer.

Lun, C. K. K., Savage, S., Jeffrey, D. J. & Chepurniy, N. 1984 Kinetic theories for granular flow: inelastic particles in Coutte flow and slightly inelastic particles in a general flow field. *J. Fluid Mech.* **140**, 223–256.

Lun, C. K. K. & Bent, A. A. 1994 Numerical simulation of inelastic frictional spheres in simple shear flow. *J. Fluid Mech.* **258**, 335–353.

Mansoorii, G. A., Carnahan, N. F., Starling, K. E. & Leland, T. W. 1971 Equilibrium thermo-dynamical properties of the mixture of hard spheres. *J. Chem. Phys.* **51**, 4319–4329.

Montanero, J. M. & Garzo, V. 2002 Monte Carlo simulation of the homogeneous cooling state for a granular mixture. *Gran. Matt.* **4**, 17–22.

van Noije, T. P. C. & Ernst, M. 1998 Velocity distributions in homogeneously cooling and heated granular fluids. *Gran. Matt.* **1**, 57–64.

Nott, P. R., Alam, M., Agrawal, K., Jackson, R. & Sundaresan, S. 1999 The effect of boundaries on the plane Couette flow of granular materials: a bifurcation analysis. *J. Fluid Mech.* **397**, 203–229.

Pöschel, T. & Luding, S. 2001 *Granular Gases*. Lecture Notes in Physics, vol. 564, Springer.

Richman, M. W. 1989 The source of second moment in dilute granular flows of highly inelastic spheres. *J. Rheol.* **33**, 1293–1304.

Savage, S. 1998 Analyses of slow high concentration flows of granular materials. *J. Fluid Mech.* **377**, 1–26.

Savage, S. & Sayed, M. 1984 Stresses developed by dry cohesionless granular materials sheared in an annular shear cell. *J. Fluid Mech.* **142**, 391–430.

Sela, S. & Goldhirsch, I. 1998 Hydrodynamic equations for rapid flows of smooth inelastic spheres, to Burnett order. *J. Fluid Mech.* **361**, 41–74.

Sela, S., Goldhirsch, I. & Noskowich, S. H. 1996 Kinetic theoretical study of a simply sheared two-dimensional granular gas to Burnett order. *Phys. Fluids* **8**, 2337–2352.

Strauss, O. 1999 Kontinuumsbeschreibung inhomogener granularer Medien. Diplomarbeit, Universität Stuttgart, Stuttgart.

Walton, O. R. & Braun, R. L. 1986 Viscosity, granular-temperature, and stress calculations for shearing assemblies of inelastic, frictional disks. *J. Rheol.* **30**, 949–980.

Willits, J. T. & Arnarson, B. Ö. 1999 Kinetic theory of a binary mixture of nearly elastic disks. *Phys. Fluids* **11**, 3116–3122.